Technische Universiteit Delft
Laboratorium voor Materiaalkunde
TMC 2

Effects of Stress Ratio and Load Frequency on The Corrosion Fatigue Crack Growth of Aluminum Alloy 5083–H321

Development of A New Test Method

Adirakhmantyo P. Hascaryantono

Supervisors:
Dr. Ir. Jan Zuidema
Ir. Saskia de Vries

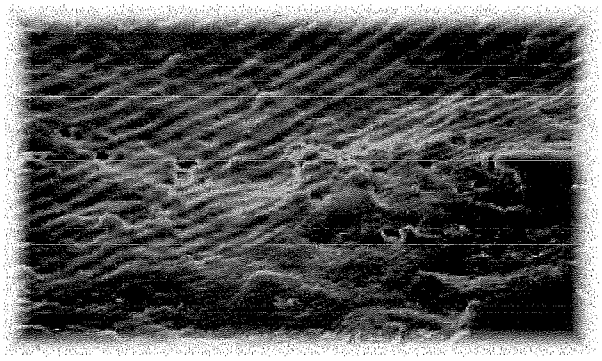

TU Delft

Section Mechanical Behavior of Materials
Materials Science and Engineering
Delft University of Technology
August 2000

Foreword

This thesis is intended to be the final report and the requirement to accomplish Master of Science Course at Department of Materials Science and Engineering, Delft University of Technology. The research was mainly carried out at Mechanical Behavior of Materials Laboratory for about six months.

Beside the knowledge that I can get from the corrosion fatigue research, there is also another important lesson that I can learn from this research, i.e.: the patience, because the test can take few days only for one specimen. However, the corrosion fatigue crack growth research is interesting because the mechanism is still not well established and not well understood. Therefore, there is a lot of new interesting things can be obtained during the research which can be read in this thesis. Hopefully, this thesis can be useful for everyone who will conduct corrosion fatigue crack growth research.

Certainly, this research would not succeed without support and help from other people. I would like to thank my supervisors, Jan Zuidema and Saskia de Vries, for their idea, critics, and directions during my research. I also would like to thank Theo van Soest for his help to use the fatigue machines, Kees van Kranenburg and Ardy Duwel for their help with the testing software, and also Bart Nobart for his little gadget but very useful for my research. Last but not least, a very great thanks to my parents, Mr. and Mrs. Soenjoto, who always support me from a very long distance.

Summary

This thesis deals with a research on the effect of stress ratio and load frequency on the corrosion fatigue crack growth in aluminum alloy 5083-H321. The specimen used in the experiment was a center-cracked-tension as explained in ASTM E647 and the environment was seawater. In order to simulate natural seawater, artificial seawater according to ASTM D1141 was used. Two orientations were used: L-T, with the crack perpendicular to the rolling direction, and T-L, with its crack parallel to the rolling direction. The research was divided into four general parts: preliminary testing, investigation of the stress ratio effects, validation of the increasing amplitude tests and investigation of the load frequency effects. The first part of the research was carried out to prepare the fatigue machines for the tests such as validation of earlier calibrations and determination of the type of seawater (aerated/anaerated or fresh/unfresh). The second part of the research dealt with the investigation of the stress ratio effect in seawater. The tests were carried out with a constant amplitude load and a frequency of 1 Hz. As a reference, a series of tests at various stress ratios in lab air was also conducted. Based on the crack growth curves of the tests in lab air, a crack closure formula was calculated. The formula was also applied to the crack growth curves in seawater, in order to see whether the effective stress intensity would be changed in seawater or not. The third part of the research was to introduce an accelerated test method and to validate the similitude of the method with the constant amplitude test in lab air and seawater. The method was actually prepared for investigation of low load frequencies. The method applied an increasing amplitude load instead of a constant amplitude load. By using this method the same stress intensity range could be achieved in shorter time. The last part of the research was to investigate the effects of load frequency on the corrosion fatigue crack growth. The tests were conducted at frequencies of 10 Hz and 1 Hz. As a comparison, a test in lab air with a constant amplitude load and an alternating load frequency from 10 Hz and 1 Hz was also conducted. Unfortunately, by applying such frequencies the tests took several days. In order to overcome this problem, the new accelerated method as described previously was applied. The main conclusion that can be inferred from the research are: the effective stress intensity does not change in seawater and the lower the load frequency the higher the crack growth rate in seawater. Furthermore, as far as corrosion fatigue crack growth behavior is concern aluminum alloy 5083-H321 is feasible for structures in seawater environment.

Contents

Nomenclature

a	crack length [mm]
a_o	notch length / initial crack length [mm]
B	specimen thickness [mm]
C, m, n	constants for Paris equation
da/dN	crack growth rate [mm/cycle]
f	frequency [Hz]
K_c	fracture toughness [MPa$\sqrt{}$m]
K_{max}	maximum stress intensity factor [MPa$\sqrt{}$m]
N	number of cycles
P_{max}	maximum load [kN]
P_{min}	minimum load [kN]
R	stress ratio
r	plastic zone size [mm]
U	crack closure formulation
U_s	crack closure formulation according to Schijve
V_x, V_y	electric potential difference [Volt]
W	specimen width [mm]
ΔK	stress intensity range [MPa$\sqrt{}$m]
ΔK_{eff}	effective stress intensity range [MPa$\sqrt{}$m]
ΔK_{th}	threshold stress intensity range [MPa$\sqrt{}$m]
ΔP	load range (see Equation 3.1) [N]
α	a/W (see Equation 3.1)
σ_{max}	maximum stress [MPa]
σ_{min}	minimum stress [MPa]
σ_{op}	opening stress [MPa]

Chapter 1

Introduction

Aluminum alloy series 5083 has been being used widely in shipbuilding for few years. The alloy provides a good combination of strength to weight ratio and corrosion resistance compared to steel alloys. Since cyclic loads due to the speed of ships are likely to happen in ship structures, an understanding of fatigue crack growth is needed. Unfortunately, unlike steel alloys, the fatigue crack growth behavior of aluminum alloys in corrosive environments is less well known. In order to understand the corrosion fatigue crack growth behavior of aluminum alloy 5083, a research in corrosion fatigue crack growth was carried out. The scope of the research is to investigate the effects of stress ratio and load frequency on the corrosion fatigue crack growth. Since this research of corrosion fatigue crack growth implies the use of low frequencies, some of the experiments will take a very long time. This is solved by introducing an accelerated test method for fatigue crack growth. In principle, an increasing amplitude load is applied to the specimen instead of a constant amplitude load. This way the experiment can be conducted in shorter time but with the same stress intensity range as in the constant amplitude load. Furthermore, to ensure that the test results are valid, several validation tests are conducted such as an investigation of the effects of seawater to the potential difference measurements, the effects of the freshness of the seawater to the crack growth rate, and the effect of the application of an accelerated load to the crack growth rate.

Before commencing the research some theoretical background related to the research is needed. The theoretical background is explained in Chapter 2 and consists of a brief theory of fatigue crack growth and corrosion fatigue crack growth. Since there is no established theory about the effects of load frequency as well as stress ratio on the corrosion fatigue crack growth, a literature review is presented instead. The theories are used to explain some findings in the experiments. Chapter 3 describes the experimental setup which is arranged especially for corrosion fatigue crack growth research. This chapter also consists of the arrangement of the corrosion cell used in the test, the test method, the data handling, and the calibration. The test procedure is also described at the end of Chapter 3. The results of all the tests are presented in Chapter 4. Then, the results are discussed and analysed in Chapter 5. In this chapter, the results are confirmed with the theory and / or compared with experiments from other researchers. Based on the discussion and analysis some conclusion and remarks can be drawn. These are described in Chapter 6.

Chapter 2

Theoretical Background

This chapter deals only with the theoretical background which is related to the experiment. The detail description about the corrosion fatigue crack growth can be read in the literature review [1]. The theory is expected to be the foundation to explain some findings from the experiment. A brief introduction about fatigue crack growth theory is described at the beginning of this chapter and followed by corrosion fatigue crack growth theory.

2.1 Fatigue Crack Growth

2.1.1 Crack Growth Rate

Cracks can propagate from notches, discontinuities, imperfections, etc. under an alternating load or fatigue load although the load is still under the yield strength and / or under fracture toughness of the material. The rate of the crack propagation / growth is material dependent. In other words, the crack growth rate behavior is unique for every material. This behavior is usually presented in a form of crack growth rates versus stress intensity range (da/dN vs ΔK) graph. A characteristic sigmoidal da/dN vs ΔK graph can be seen in Figure 2.1. The curve can be divided into three regions [2]. In region I, there is a threshold value, ΔK_{th}. Below this value cracks do not grow. Above this value the crack growth rate increases rapidly with increasing ΔK. In region II, the relation between stress intensity range with crack growth rate is log-log linear. In the region III, the crack growth curve increases towards an asymptote where the maximum stress intensity factor, K_{max}, is equal to the critical stress intensity factor, K_C. The crack growth curve in the region II can be approximated by Paris equation as expressed in Equation 2.1.

$$da/dN = C(\Delta K)^m \tag{2.1}$$

where,

da/dN = crack growth rate
C, m = constants which are empirically determined
ΔK = stress intensity range

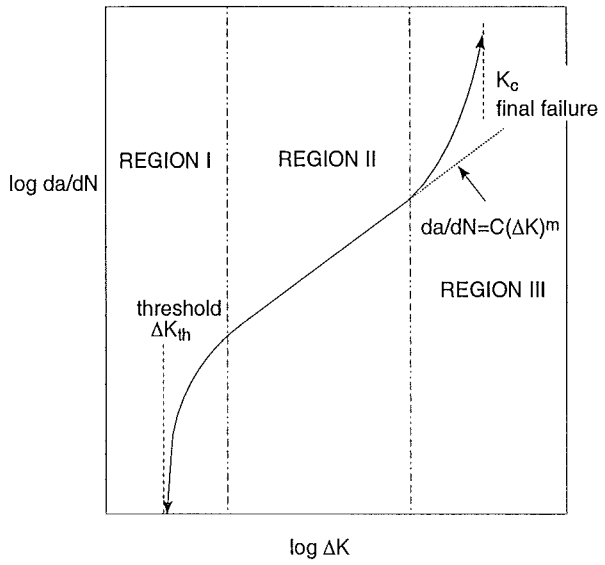

Figure 2.1: A typical crack growth curve da/dN vs ΔK[2].

2.1.2 Crack Closure

Effects of crack closure are prominent when the stress ratio, ($R = \sigma_{min}/\sigma_{max}$) applied to a specimen is low or even negative. The presence of the crack closure can reduce the crack growth rate. Actually, crack closure occurs as a consequence of crack tip plasticity on the crack flanks and surface roughness caused by shear lips [3]. However, for the sake of simplicity, only the crack tip plasticity is considered in the following explanation. As an alternating load is applied on a cracked material, the crack closure takes place as described in Figure 2.2 [2]. This gives a wedging effect on the crack surfaces during unloading cycles. In other words, the crack is already closed before the minimum load is reached. Such a condition leads to a reduction of ΔK to a certain level, ΔK_{eff} (see Figure 2.2). The minimum stress level at which the crack start to open is called the opening stress, σ_{op}. Consequently, if the minimum stress of an alternating load is equal to σ_{op} (i.e.: stress ratio, R, is high enough) the crack closure has no effect at all. Moreover, different stress ratios can result in the same crack growth rates (da/dN) as long as ΔK_{eff} is the same.

Based on the previous explanation, the effective stress intensity range, ΔK_{eff}, is a function of the stress ratio (R) at the same ΔK level. Thus, the crack growth rate, da/dN, is also a function of the stress ratio (see Equation 2.2). The effect of stress ratio on the crack growth rate curve is illustrated in Figure 2.3(a) [4]. Several attempts have been made to determine the relation (U) between ΔK_{eff} and R. One of the well known formulations is Schijve's equation (U_S) as

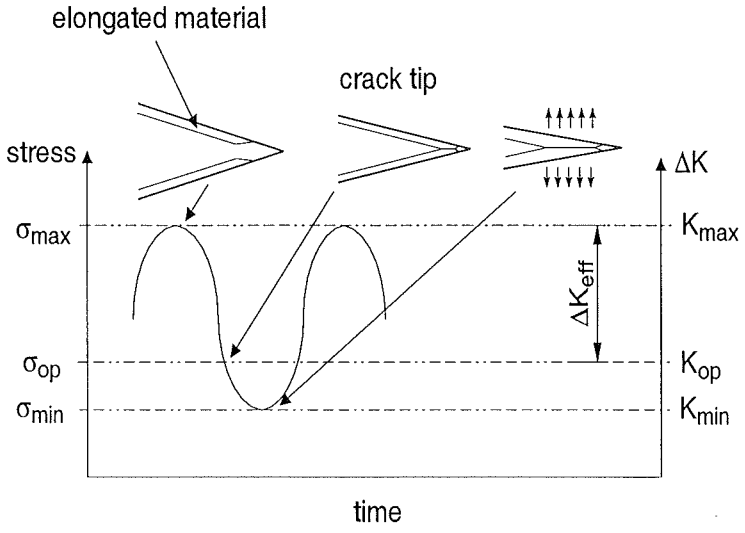

Figure 2.2: Crack closure effects on stress intensity range (ΔK) [2].

expressed in Equation 2.2.

$$\begin{aligned} da/dN &= C(\Delta K_{eff})^n \\ \Delta K_{eff} &= U_s.\Delta K \\ U_s &= 0.55 + 0.35R + 0.1R^2 \end{aligned} \tag{2.2}$$

where,

C, n = constants
ΔK_{eff} = effective stress intensity range
R = stress ratio

As a consequence of the previous equation, several combinations of R and ΔK can result in the same da/dN curve. For example, by applying Schijve's equation, Figure 2.3(a) can be represented as da/dN vs ΔK_{eff} instead of da/dN vs ΔK as seen in Figure 2.3(b).

2.1.3 Crack Growth in Transition Region

When cracked structures are subjected to variable amplitude load, the behavior of fatigue crack growth is quite complicated. This is due to the change of the load amplitude from one level to another one. The transition effect of the load can be illustrated as in Figure 2.4 [5]. In the transition region where the load amplitude changes, the opening stress (σ_{op}) needs some time to change to the new level. In the step-down loading this leads to decrease ΔK_{eff} and results in crack growth retardation during the transition (see Figure 2.4(a)). The crack growth retardation

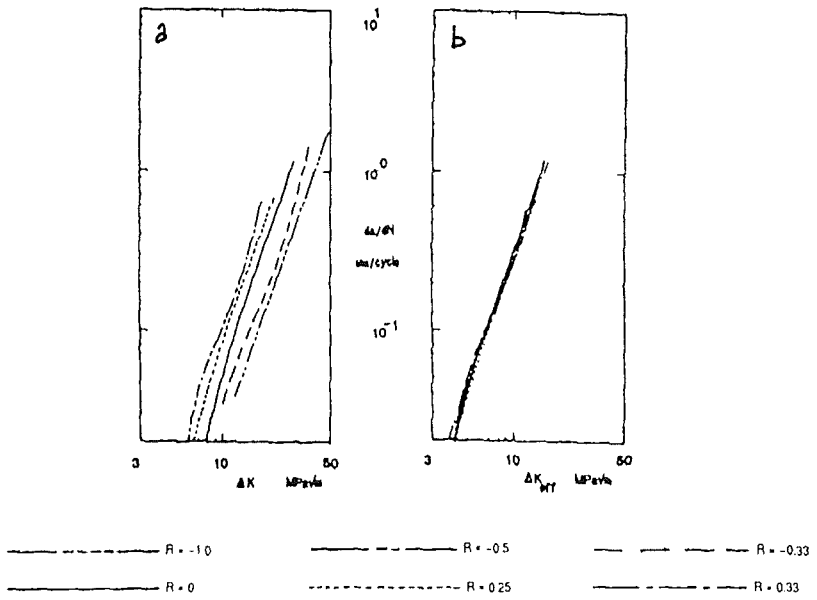

Figure 2.3: (a) Effects of stress ratio on crack growth curves (b) Crack growth curve as a function of effective stress intensity range (ΔK_{eff}).[4].

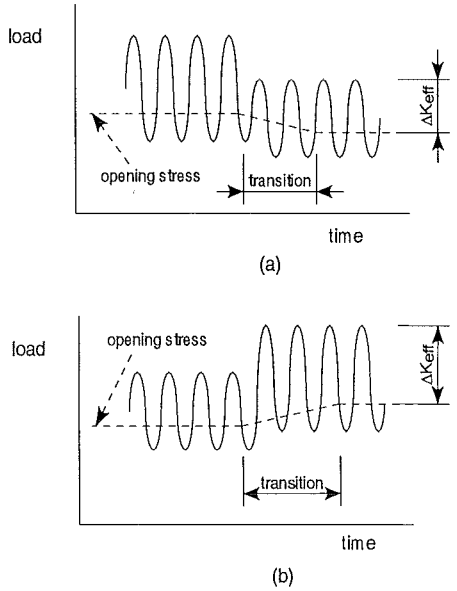

Figure 2.4: Transition effects due to the change in load level:(a) Step down loading (b) Step up loading [5].

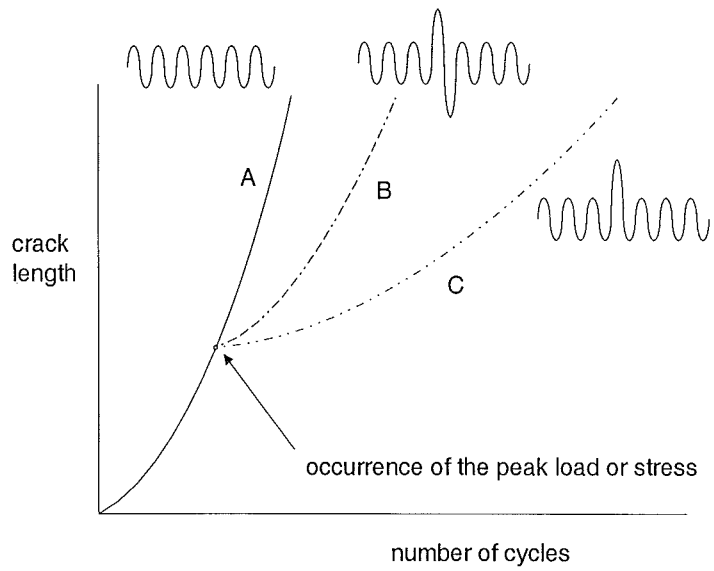

Figure 2.5: Crack growth curves with a constant amplitude load and a constant amplitude load with a peak load [2].

will be explained further in the next sub-section. In the step-up loading ΔK_{eff} increases and results in the crack growth acceleration during the transition (see Figure 2.4(b)) before it returns to the normal level.

2.1.4 Crack Growth Retardation

One peak load during a long period of a constant amplitude loading can result in crack growth retardation. For example, a specimen is subjected to a cyclic load as illustrated in Figure 2.5. A positive peak load (curve C) and a positive-negative peak load (curve B) are given during the constant amplitude loading. As a result, the crack growth rate curve will change as illustrated in Figure 2.5 [2]. There is a significant retardation in the crack growth compared to the constant amplitude crack growth curve (curve A). However, the retardation effect is greater in the positive peak load compared to the positive-negative load. This is attributed to the plastic zone size at the crack tip, which will be explained here.

At curve C, the positive peak load first gives a higher crack growth rate because ΔK then becomes larger. Besides that, the minimum stress (σ_{min}) can be somewhat higher than the opening stress (σ_{op}). As a consequence, ΔK_{eff} can be higher than before and result in a higher crack growth rate. Then, after the load is back to normal the crack growth is retarded. This is because of the presence of the large plastic zone size at the crack tip which is formed during the positive peak load. Since the plastic zone is in high residual compressive stress, the crack propagation in the plastic zone is retarded. Also a wake of enhanced residual deformation forms behind the

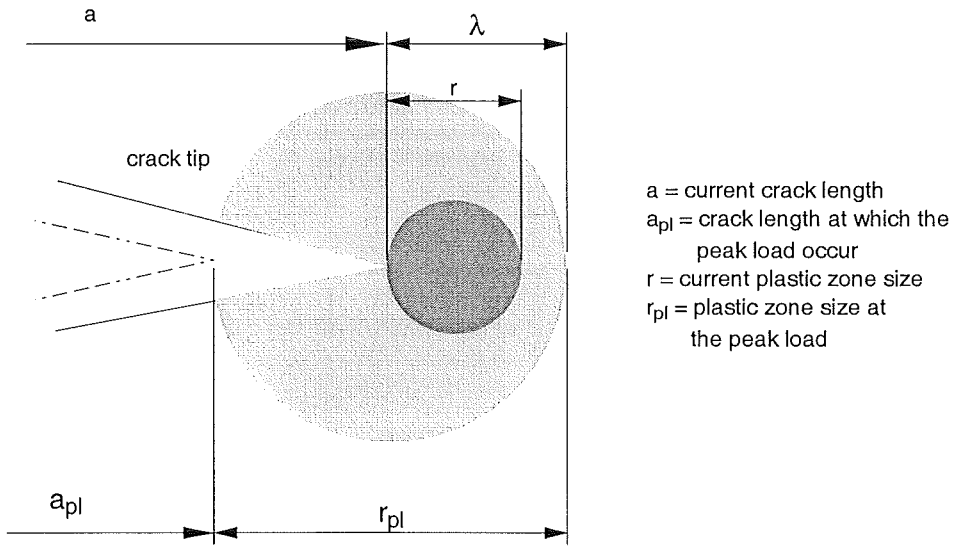

Figure 2.6: Wheeler retardation model [2].

crack tip and causes an increase in crack closure [2]. As soon as the crack tip leaves the plastic zone, then the crack growth is back to normal again.

At curve B, a positive-negative peak load is applied during a constant amplitude load. The negative peak stress reverses most of the tensile plastic deformation due to the positive peak stress and leads to a reduction of the retardation effects (see Figure 2.5). In order to determine the crack growth retardation quantitatively, Wheeler suggested a retardation model as seen in Figure 2.6 [2]. As long as the plastic zone size due to the normal load (r) remains within the plastic zone size due to the peak load ($r < \lambda$), the crack growth is still retarded. When $r \geq \lambda$ the crack growth returns to normal again.

2.2 Corrosion Fatigue Crack Growth Mechanisms in Aluminum Alloys

There is no well established theory for corrosion fatigue crack growth mechanism in aluminum alloys. However, some researchers have suggested some mechanism theories. The theories are explained in the following sub-sections. These three theories are the most accepted theories among the others.

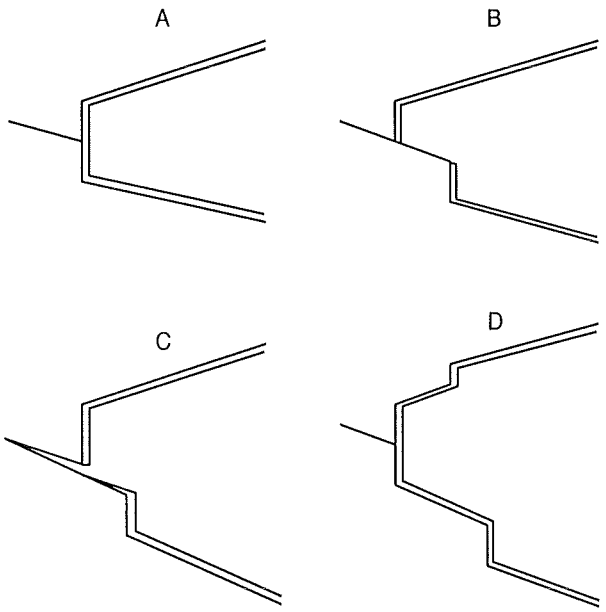

Figure 2.7: Sequence of anodic dissolution at the crack tip [6].

2.2.1 Anodic Dissolution Mechanism

Anodic dissolution mechanisms are also known as active path dissolution, slip dissolution, strain/ stress enhanced dissolution, and surface film rupture/metal dissolution. This theory suggests that crack growth rates are enhanced by anodic dissolution along susceptible paths such as grain boundaries or crack tip strained metal which can be relatively anodic to the surrounding matrix. In corrosion fatigue cracking, the anodic dissolution mechanism depends on the rupture of the protective film at the crack tip by the fatigue process and the subsequent repassivation of the fresh metal surface. Corrosion fatigue crack growth rates will be controlled by the bare surface anodic dissolution rate, the rate of repassivation, the rate of oxide film rupture, the mass transport of reactant to the dissolving surface, and the flux of solvated metal cations away from the surface. The repassivation process must be rapid enough to avoid extensive and widespread dissolution which can lead to crack tip blunting and pit formation instead of sharp and directional crack advance. However, it must be slow enough to allow significant dissolution at the crack tip [6].

The sequence of the anodic dissolution is described in Figure 2.7. Under tensile fatigue loading, a slip step is formed at the crack tip and destructs the protective surface film as seen in Figure 2.7A - B. The freshly created surface reacts with the environment and partly dissolves until the crack tip region is completely repassivated and the protective surface film is repaired (Figure 2.7C - D). The processes repeat themselves when a slip step destructs the protective film again and exposes more bare surface.

This theory has been applied successfully in aqueous environment, but it can not explain the corrosion fatigue mechanism in gaseous environment such as water vapor, hydrogen, or hydrogen

sulfide. It also fails to be applied in deaerated distilled water where the electrochemical reaction necessary for dissolution at the crack tip is unattainable.

2.2.2 Hydrogen Assisted Mechanism

Hartman [7] suggested that the cause of the large increase in the rate of crack growth by water is the formation of hydrogen gas with high pressure in the region ahead of the crack tip, driven in by the reaction of water with the freshly created aluminum crack surfaces [8]. The reaction sequence for aluminum alloys can be expressed by the following reactions [9],

$$\begin{aligned} 2Al^{3+} + 3H_2O &\longrightarrow Al_2O_3 + 6H^+ \\ 6H^+ + 6e^- &\rightleftharpoons 6[H] \end{aligned} \tag{2.3}$$

and,

$$H_2 \rightleftharpoons 2[H] \tag{2.4}$$

Based on these facts, the mechanism of corrosion fatigue in aluminum alloys is believed to result from hydrogen embrittlement in conjunction with the mechanical driving force for crack growth. The process is illustrated in Figure 2.8 [9]. The free hydrogen atoms produced by chemical reactions at the crack tip (Equations 2.3, 2.4, and Figure 2.8 step 1) are driven from the metal surface layers of the crack tip to various internal destinations in the microstructure (Figure 2.8 step 2). This process is governed by classical lattice diffusion, or by dislocation transport of hydrogen atoms, or both. Under cyclic loading, hydrogen atoms in the matrix lattice will segregate to inhomogeneities, such as grain boundaries, matrix/constituent particle interfaces, or (locked) dislocations, depending upon which sites provide the highest binding energy with hydrogen (Figure 2.8(c)). When the local hydrogen concentration exceeds the limit of solubility, hydrogen-filled microvoids nucleate easily. Then the microvoids at the crack tip will coalesce and enhance the fatigue crack propagation.

2.2.3 Surface Adsorption Mechanism

A recent study by Petit [10] shows that two different mechanisms occur in the corrosion fatigue crack propagation of aluminum alloys. In the stage I crack growth, the hydrogen assisted mechanism as described in the previous sub-section is dominant, but in the stage II (Paris regime) the adsorption assisted propagation occurs. The species which are adsorbed by a metal surface, can be water molecules or other gases. The physical adsorption of water, for example, would thus induce a lower value of the energy required to create a unit crack surface area. Moreover, pure adsorption (i.e. without any penetration of active species in the bulk material) can seriously alter the mechanical resistance of material [11].

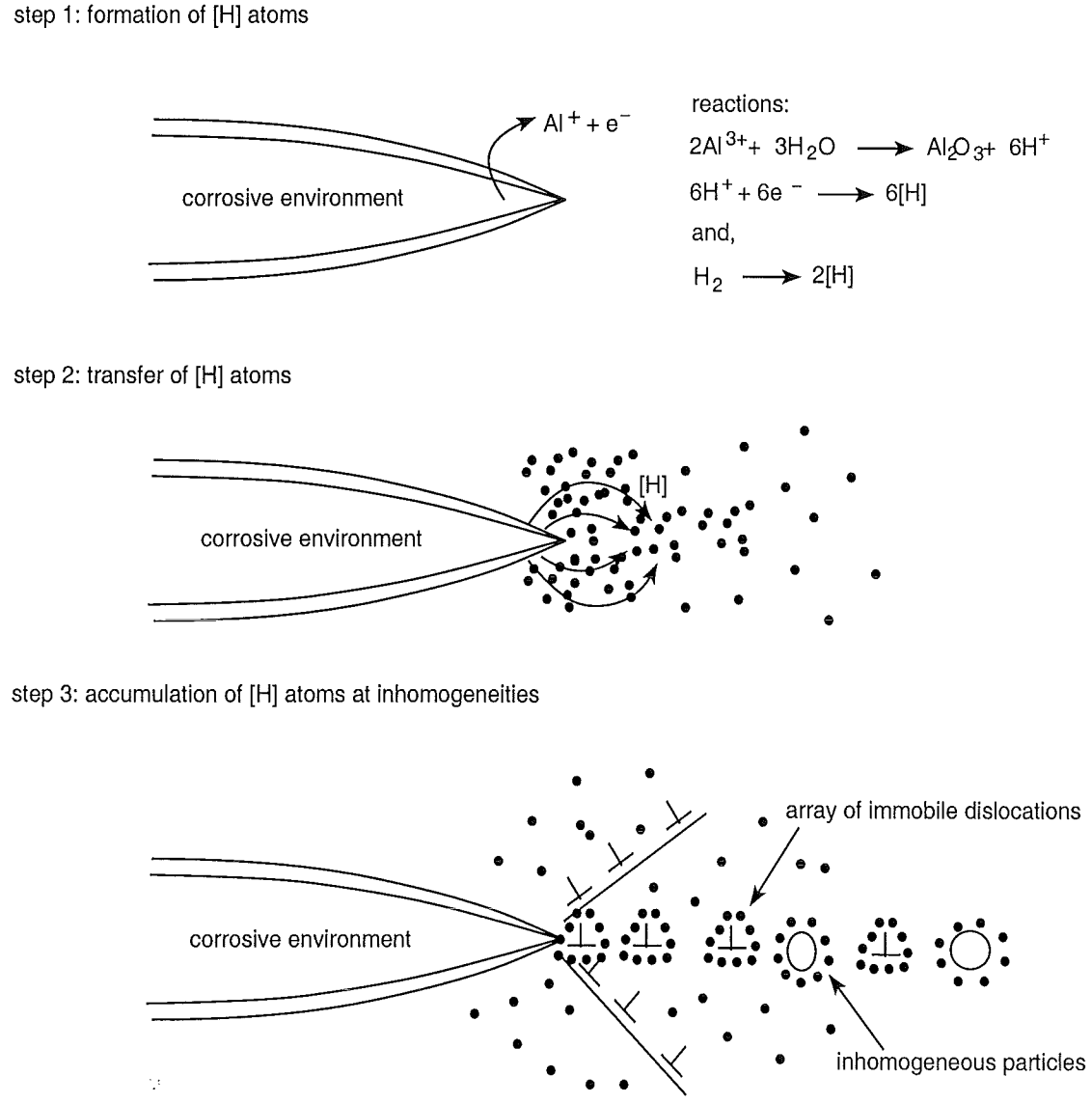

Figure 2.8: Schematic representation of a mechanism for corrosion-fatigue crack propagation due to hydrogen embrittlement [9].

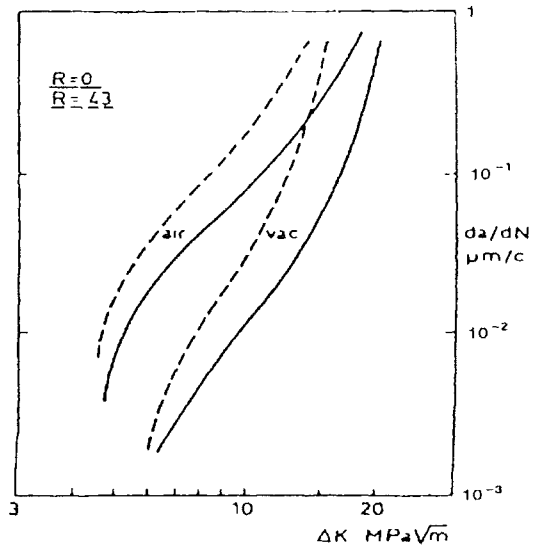

Figure 2.9: Fatigue crack growth data obtained by Enochs and Devereux for 5052-H34 aluminum alloy in air and vacuum at two different R-values (0 and 0.43) [12].

2.3 Effects of Stress Ratio on Corrosion Fatigue Crack Growth

The stress ratio, R, is associated with the crack closure effect, since it determines the range of effective stress intensity factors, ΔK_{eff}. The effect of fatigue load ratio is observed in all type of environments, because plastic deformation always occurs on the crack tip surface of aluminum alloys. Figure 2.9 shows the effect of stress ratio on the corrosion fatigue crack growth for aluminum alloy 5052-H34 [12]. The experiment was carried out in air and vacuum, and the stress ratios used in this experiment were R = 0 and R = 0.43. Both results (in air and vacuum) show that the higher crack growth rates were achieved at the higher stress ratio (Figure 2.9). These results are theoretically expected, since the higher stress ratio leads to a larger ΔK_{eff}. This causes higher crack growth rates. The result also shows that the effect of the environment is still comparable. In other words, the shape of the curves in both environment is the same, they are only shifted.

However, a study by Ewalds et al. [4] showed that the effect of stress ratio (crack closure) on crack growth rates could not always be compensated by Schijve's formula as expressed in Equation 2.2. It was demonstrated by one of the experiments that was conducted in air-saturated seawater at various stress ratios. The corresponding crack growth curves can be seen in Figure 2.10. The compensation for crack closure in air-saturated seawater does not give enough reduction in ΔK (especially in negative R). This enhanced crack closure can be explained by the fact that the crack opening stress, σ_{op}, in such an environment, for some reason, is higher than in other environments. The fractographic observations strongly suggest that the cause could be owing to corrosion product wedging on the crack surfaces. Examination of the specimens in

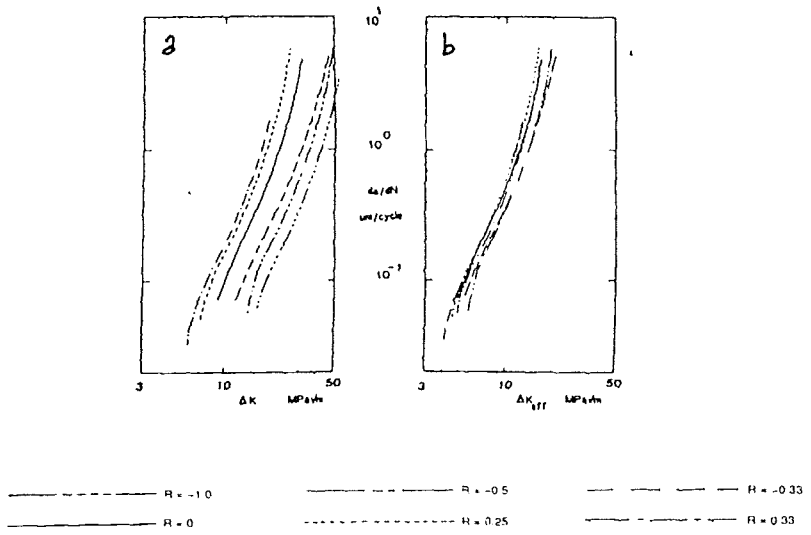

Figure 2.10: Fatigue crack growth rates for 2024-T3 in air-saturated seawater (a) da/dN versus ΔK (b) da/dN versus ΔK_{eff} according to Schijve [4].

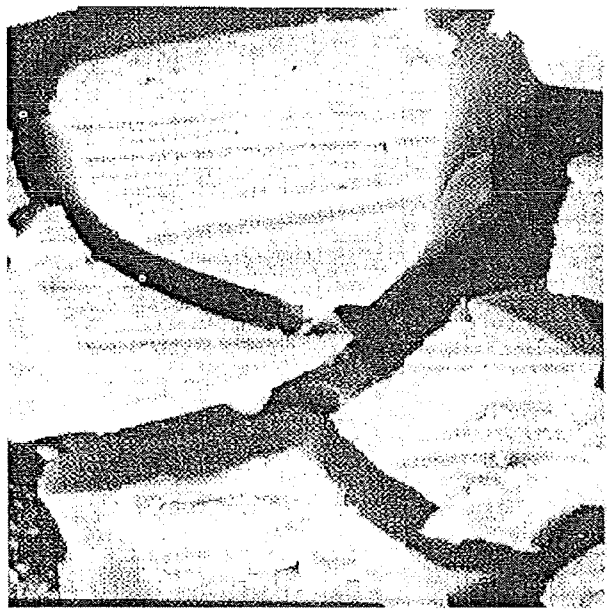

Figure 2.11: Mud crack pattern on crack surface fatigued in air-saturated seawater at R=0 (magnification x3000) [4].

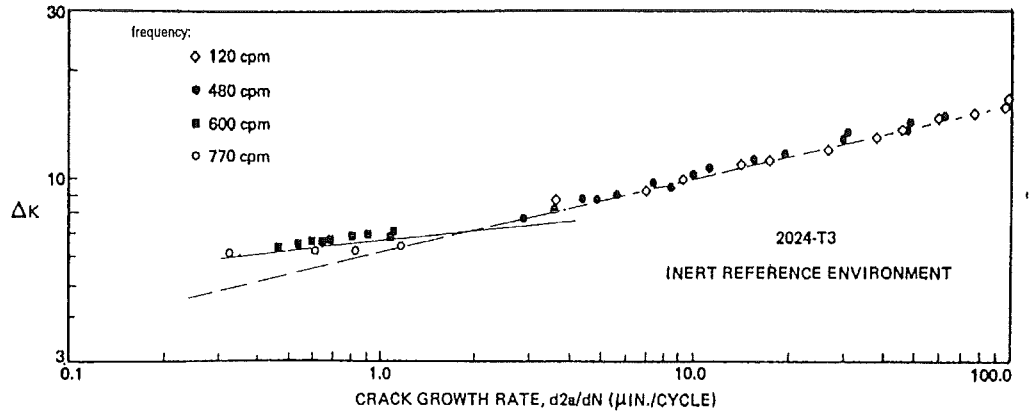

Figure 2.12: Fatigue crack growth rate (ΔK vs d2a/dN) for 2024-T3 tested in dessicated argon (less than 2 ppm H_2O) [13].

a SEM shows that after fatigue in air-saturated seawater the fracture surfaces are partly overlaid with patches of corrosion product exhibiting 'mud crack patterns' as seen in Figure 2.11. This appearance is typical of relatively thick layers of corrosion product which shrank and cracked during drying. Scratch marking which is superimposed on the crack mud pattern can also be seen in the photograph. This indicates that the relatively thick corrosion layer was compressed between the crack surfaces. This corrosion product wedging causes an increase of the threshold stress intensity for crack growth and in turn increases the crack opening stress, σ_{op}.

2.4 Effects of Load Frequency on Corrosion Fatigue Crack Growth

In considering the effect of test frequency, it is important to distinguish between that which is 'intrinsic' to the material (i.e. rate-sensitivity of the material) and that which belongs to environmental effects. Experimental evidence showed that there is essentially no intrinsic frequency effect for most high strength structural metals over a range of test frequencies; the frequency effect is strictly related to environment interactions. This was proven with the experiment of 2024-T3 aluminum alloy in dessicated argon by Feeney et al. [13] as seen in Figure 2.12. The experiment was carried out in test frequencies of 120 cpm (cycles per minute), 480 cpm, 600 cpm, and 770 cpm. Figure 2.12 shows that the transition in crack growth rates is intrinsically material behavior.

However, the crack growth rate in corrosive environments is strongly dependent on the loading frequency. Theoretically, lower frequencies give enough time for the reaction between aluminum alloys and environments. Consequently, the lower the loading frequency the higher the crack growth rates. This was confirmed by Holroyd and Hardie [14]. The experiments were carried out

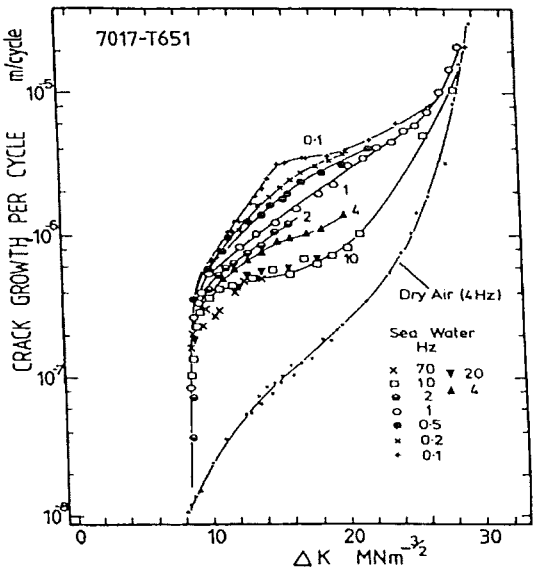

Figure 2.13: Crack growth rates during fatigue of 7017-T651 in dry air at 4 Hz and in seawater at frequencies from 0.1 to 70 hz, as a function of ΔK [14].

in fresh unpolluted natural seawater with a pH of 8.1 to 8.3 and a temperature of 25$\pm$2 ^{0}C. The aluminum alloy 7017-T651 was tested under 0.1 to 70 Hz fatigue loads. As a reference, crack growth data in an inert environment was obtained from tests in dry air (complete immersion in anhydrous magnesium perchlorate) at 4 Hz. The waveform used in the tests was triangular with a stress ratio (R) of 0.1. The results can be seen in Figure 2.13 which shows a decrease in influence of the corrosive environment with increasing test frequencies.

2.5 Increasing Amplitude Crack Growth Test

As explained in the previous sections, the effect of corrosive environments is larger as the loading frequencies are lower. Unfortunately, tests in lower frequencies such as 0.1 Hz or lower will take a very long time. During the long test, disturbances can occur to equipment and/or specimens. To overcome this problem, an accelerated test is introduced in this research. In the conventional method, the crack growth test is conducted with a constant amplitude load and the stress intensity range (ΔK) gradually increases as a function of crack length (see Figure 2.14). If the constant amplitude method is applied for the low frequency test, it will be time consuming. However, the same ΔK range as in the constant amplitude method can be achieved faster by increasing the load amplitude during the test. The comparison between the constant amplitude (CA) and the increasing amplitude (IA) tests is illustrated in Figure 2.14.

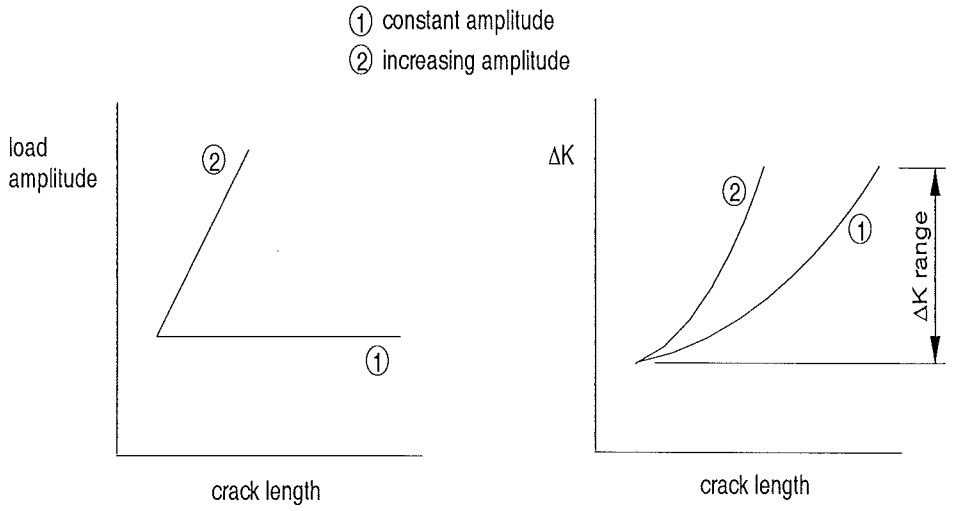

Figure 2.14: Comparison between CA and IA tests.

Chapter 3

Experimental Setup

3.1 Specimen

The specimen used in the experiment was aluminum alloy 5083-H321 with the composition as presented in Table 3.1. The temper designation, H321, means that the material was strain hardened and stabilized with an amount less than that of H32 temper. The geometry of the specimen was a standard Center Cracked Tensile (CCT) specimen according to ASTM E647 [15]. The important dimensions of the specimen were 8 mm of thickness (B) and 100 mm of width (W). The notch length (a_o) was 5 mm. The complete dimensions of the specimen can be seen in Appendix A1. There were two types of the specimens, i.e.: L-T (the specimen length is parallel with the rolling direction) and T-L (the specimen length is perpendicular to the rolling direction).

3.2 Seawater

In order to simulate the corrosion fatigue crack growth process in seawater environment, artificial seawater was used. By using the artificial seawater, reproducible tests could be achieved. During the experiment, aerated and anaerated seawater were used. The seawater was prepared according to the Substitute Ocean Water ASTM D1141 (without heavy metals) and explained completely in Appendix A2 [16]. The chemical composition of the seawater is given in Table 3.2. The pH of the seawater was adjusted to 8.2 with 0.1 M NaOH. The seawater was stored in a tank and circulated through a corrosion cell that was attached to the specimen. The amount of the seawater used in the circulated system was 20 litres. A detailed description of the corrosion cell and the equipment arrangement are presented in Section 3.4 and 3.5. To ensure that the seawater used in the experiment was always fresh and not degraded, the seawater was replaced completely every week. The temperature of the seawater was not controlled, but it was ranging from 21 - 24 ^{0}C.

Table 3.1: Alloy composition of 5083-H321 (taken from *www.matweb.com*).

Element	Al	Mg	Mn	Fe	Si	Zn	Cr	Ti	Cu
Weight %	94.8	4 - 4.9	0.4 - 1	max 0.4	max 0.4	max 0.25	0.05 - 0.25	max 0.15	max 0.1

Table 3.2: Chemical composition of substitute ocean water.

Compound	Concentration, g/L
NaCl	24.53
$MgCl_2$	5.20
Na_2SO_4	4.09
$CaCl_2$	1.16
KCl	0.695
$NaHCO_3$	0.201
KBr	0.101
H_3BO_3	0.027
$SrCl_2$	0.025
NaF	0.003

3.3 Crack Length Measurement

Crack length was measured with the electric potential difference technique. This technique relies on the principle that the electric field in a cracked specimen with a current flowing through it is a function of the specimen geometry, and in particular the crack size. For a constant current flow, the electric potential across the crack plane will increase with increasing crack size due to modification of the electrical field and associated perturbation of the current streamlines [15]. The change in voltage can be related to crack length through an experimental calibration relationship. However, the potential difference technique used in the experiment was a bit different compared to ASTM E647. In the experiment, two potential differences were measured instead of one. The lay out of the crack length measurement can be seen in Figure 3.1. Then, the ratio of these potentials $(10 * V_x/V_{y)}$ was related to the crack length (a) with an order three polynomial. Since there were two types of specimens, i.e.: T-L and L-T specimens, two calibration curves were needed. The calibration was carried out at a constant ΔK of 7 MPa$\sqrt{\text{m}}$ and a frequency of 10 Hz. The result of the calibration is presented in Figure 3.2. Obviously, there is no significant difference in the calibration curves between these two types of specimens. The calibration was carried out only in lab air although the calibration curves were used also in the artificial seawater. However, the presence of the seawater did not affect the crack length measurement, since the resistance of the seawater is far greater than the aluminum alloy. This assumption was confirmed by a visual measurement which will be explained in Chapter 5.

3.4 Corrosion Cell

The corrosion cell was made of plexiglass, so that the crack advance could also be observed visually. It was designed to facilitate a corrosive environment at the crack tip. Only the part where the crack would grow was covered by the cell. The layout of the cell attached to the specimen can be seen in Figure 3.3. The detail dimensions of the corrosion cell are given in Appendix A3. It can be seen in Figure 3.3 that only the lower wall was attached to the specimen,

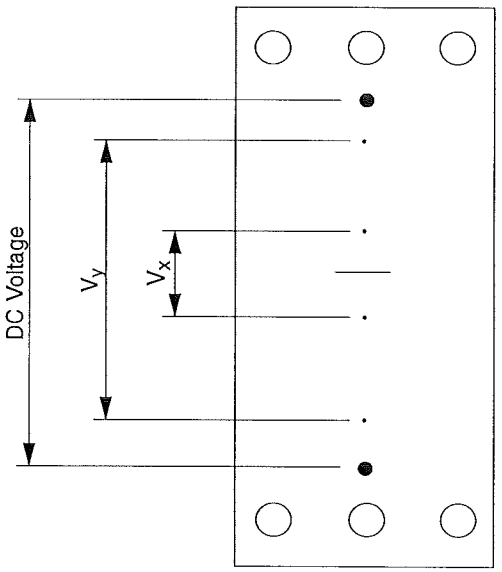

Figure 3.1: Layout of the potential difference technique.

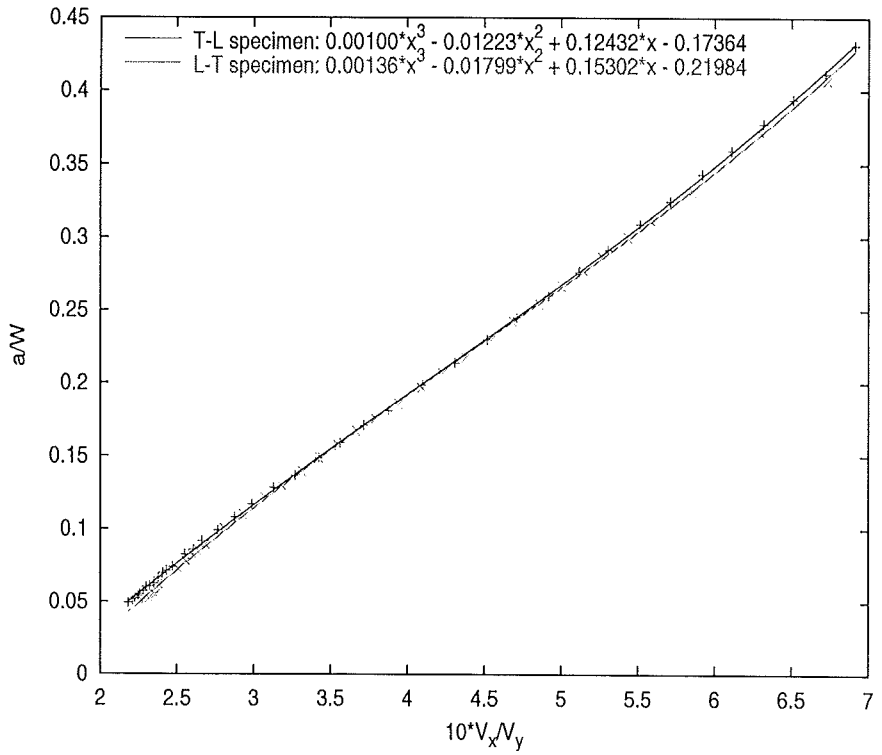

Figure 3.2: Calibration curves of two types of the specimens at Schenck machine.

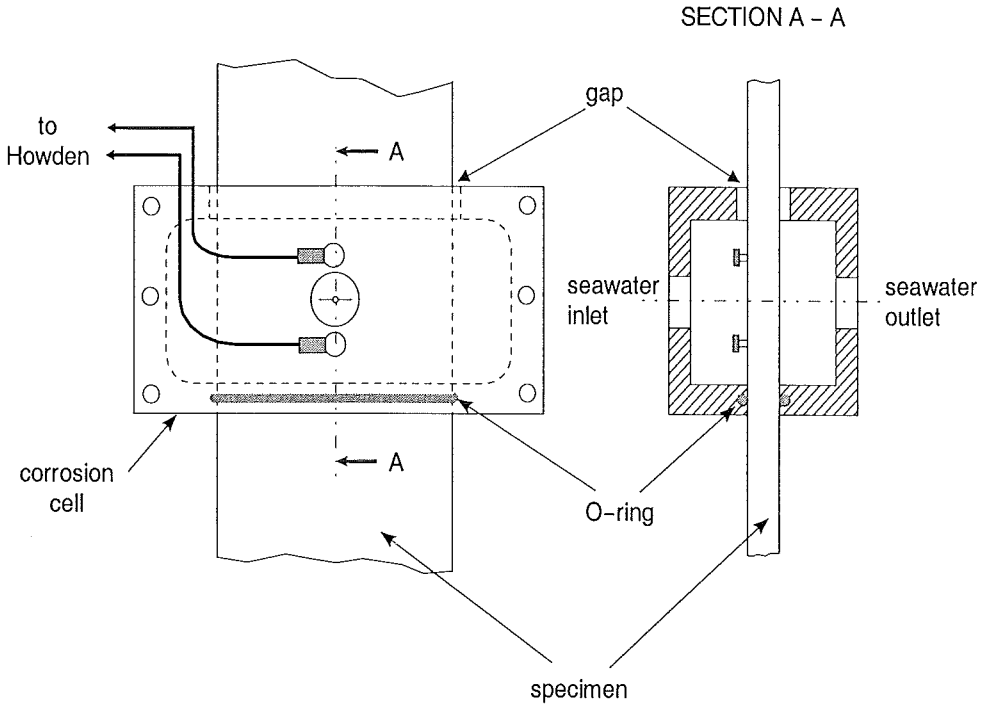

Figure 3.3: Layout of the corrosion cell.

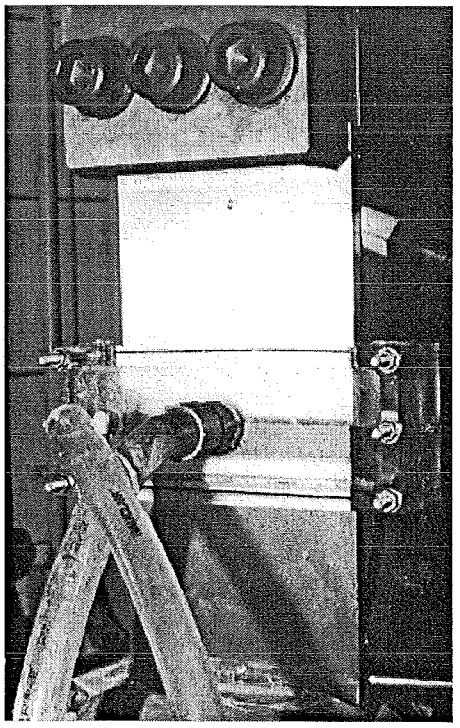

Figure 3.4: A front view of the specimen with the corrosion cell attached.

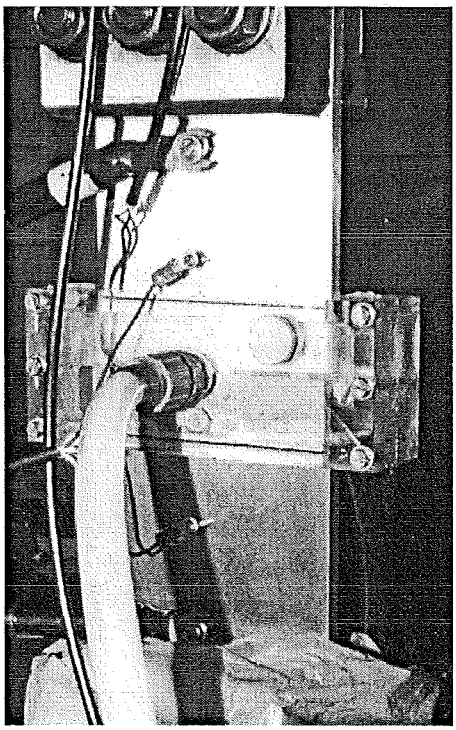

Figure 3.5: A rear view of the specimen with the corrosion cell attached.

whilst the upper one was free. This was intended to ensure that no load would be transferred to the cell or absorbed by the cell. In order to avoid the leakage, silicon rubber was used to seal the cell. Photographs of the corrosion cell attached to a specimen can be seen in Figure 3.4 and Figure 3.5.

3.5 Complete Layout

A schematic layout for the corrosion fatigue crack growth test is described in Figure 3.6. The fatigue machines used in the experiment were SCHENCK HYDROPULS (250 kN) and MTS 810 (100 kN). The load of the machines was controlled by a load table in the PC. The electric potential difference was measured by Howden as seen in Figure 3.6. The DC voltage was also supplied by Howden. Then, the output of Howden ($10 * V_x/V_y$) was recorded by a PC. The seawater was circulated by a pump to the corrosion cell from the tank (see Figure 3.6). The seawater flow rate was maintained at maximum 7 mL/sec, by adjusting the valve (V_1). This range was chosen because it could give a constant seawater level in the corrosion cell. Above 7 mL/sec, the seawater would flow out the cell, because the upper wall of the cell was open. In order to achieve good reproducibility during the experiment, the valve was adjusted to produce a flow rate between 5 - 7 mL/sec. The valve V_2 was only used for a maintenance purpose. An aerated seawater condition was created by bubbling air into the seawater (see Figure 3.6), whilst disconnecting the air pump provided an anaerated condition.

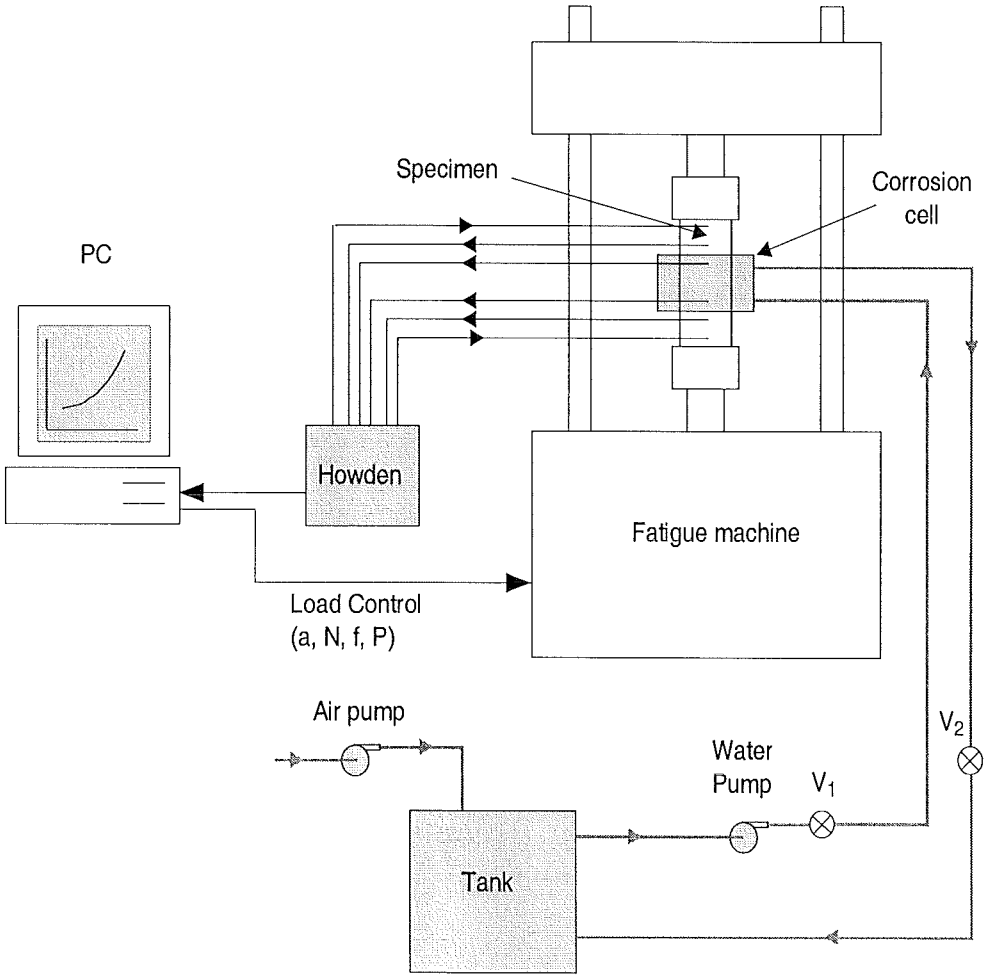

Figure 3.6: A schematic layout of the corrosion fatigue crack growth test.

3.6 Data Handling

Data obtained from the test were crack length versus cycles (a vs N) with the corresponding load and frequency. Then the data were processed to create a crack growth rate versus stress intensity factor range curve (da/dN vs ΔK). According to ASTM E647 [15], there are two recommended method to convert the data from a vs N to da/dN vs ΔK, i.e.: the secant method and the incremental polynomial method. In the experiment the incremental poynomial method was used. Since the data obtained from the test were usually scattered or fluctuated, there was a possibility that da/dN values could be negative. This was not correct because a crack length should always increase. In order to overcome this problem, data reduction was applied before creating the da/dN vs ΔK curve. The idea behind the data reduction was to select data points at certain crack lengths. This way, always increasing crack length data with increasing number of cycles could be obtained. Thus, avoiding negative da/dN values which usually caused by fluctuation of the potential difference measurement. The technique is illustrated in Figure 3.7. Besides da/dN values, the stress intensity range (ΔK) must be also determined. The formulation used to calculate ΔK was obtained from ASTM E647 [15] which is expressed in Equation 3.1.

$$\Delta K = \frac{\Delta P}{B}\sqrt{\frac{\pi\alpha}{2W}\sec\frac{\pi\alpha}{2}} \tag{3.1}$$

or,

$$\Delta K = \Delta\sigma\sqrt{\pi a \sec\frac{\pi a}{W}} \tag{3.2}$$

where,

$$\begin{aligned} \Delta P &= P_{max} - P_{min} \\ \Delta\sigma &= \sigma_{max} - \sigma_{min} \\ \alpha &= 2a/W \\ B &= thickness \\ W &= width \end{aligned}$$

The listing of the incremental polynomial program as well as the screenshot can be seen in Appendix A4. The main program is taken from ASTM E647 and has been modified to fulfil our needs.

3.7 Test Procedures

Several tests were conducted in the experimental work. However, the detailed test parameters for each specimen are not given in this section; they are listed in Appendix A5. The experimental work was divided into four parts as described into the following Sub-sections.

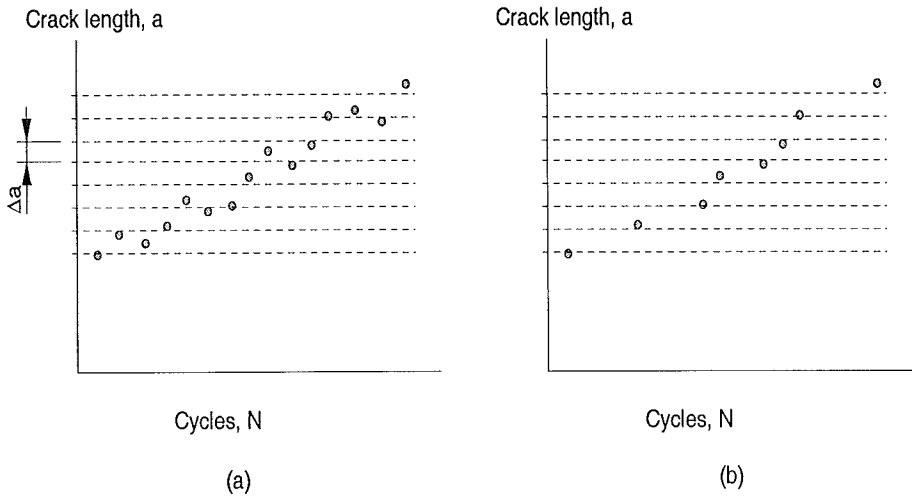

Figure 3.7: (a) Data are divided into several crack lengths (b) Nearest data points to the determined crack lengths are selected.

3.7.1 Preliminary Testing

The preliminary tests included validation of earlier calibrations and an investigation of the effects of the seawater conditions.

Validation of Calibration for MTS Machine

The MTS machine as well as the SCHENCK machine was used in the experiments. For practical reason, the calibration curves which presented in Figure 3.2 were used. Since the calibration was done at the SCHENCK machine, a validation was needed. The validation was conducted by comparing crack growth curves at R = -1 and a frequency of 10 Hz with constant amplitude (CA) load from two machines.

Validation of Calibration in Seawater

Since an electric potential difference method was used (with Howden equipment) to measure the crack length, there was a possiblity that the presence of the seawater would affect the crack length measurement. However, it was difficult to make a calibration curve in seawater environment. This was due to the lack of visibility when the corrosion cell was attached to the specimen (see Figure 3.4 and 3.5). Therefore, the calibration curve in lab air was used instead. In order to ensure that the curve was also valid for seawater, a validation was needed. It was necessary to know if the applied electric current was transmitted also in the seawater or not, and in turn to affect the potential reading of Howden equipment and also the corrosion crack growth mechanism. The validation was carried out by comparing crack growth curves between visual measurement and electric potential difference (Howden measurement) at a frequency of 1 Hz and R = 0.1. The visual measurement was carried out without installing the Howden equipment, hence there was

no electric potential applied to the specimen. The visual measurement only resulted in a few data points because it obviously could not be done continuously. Since only a few number of data resulted from the visual measurement, the crack growth rate calculation used in the test was secant method [15].

Investigation of The Use of Fresh/Unfresh Seawater

One CA test in fresh seawater and another one in unfresh seawater were carried out for this investigation. The fresh seawater was seawater which had never been used for tests before, whilst the unfresh seawater had been used for tests for three weeks. Both tests were conducted in anaerated seawater at R = 0.1 and a frequency of 1 Hz.

Investigation of The Use of Anaerated/Aerated Seawater

For this investigation, one CA test in anaerated seawater and another one in aerated seawater were carried out. The aerated condition was made by bubbling air into the seawater. Both tests were conducted at R = 0.1 and a frequency of 1 Hz.

3.7.2 Effects of Stress Ratio

The goal of the experiments was to investigate whether a seawater environment changed the crack closure behavior or not.

Tests at Various Stress Ratios in Lab Air

These tests were conducted to provide crack growth references before commencing corrosion fatigue crack growth tests. The tests were conducted with constant amplitude load at a frequency of 10 Hz and stress ratios of -1, -0.25, 0.1, 0.5, and 0.7. The specimens used in these tests were T-L and L-T specimens. The detailed test parameters of every specimen can be seen in Appendix A5.

Tests at Various Stress Ratios in Seawater

A series of tests at various stress ratios was carried out in order to investigate if there was a change in closure effect due to the corrosion process or not. The tests were conducted with a constant amplitude load at R = 0.1 and R = 0.5 and a frequency of 1 Hz. The tests were conducted twice for every stress ratio.

3.7.3 Increasing Amplitude (IA) Tests

The aim of the tests was to validate the increasing amplitude (IA) test with the constant amplitude (CA) test.

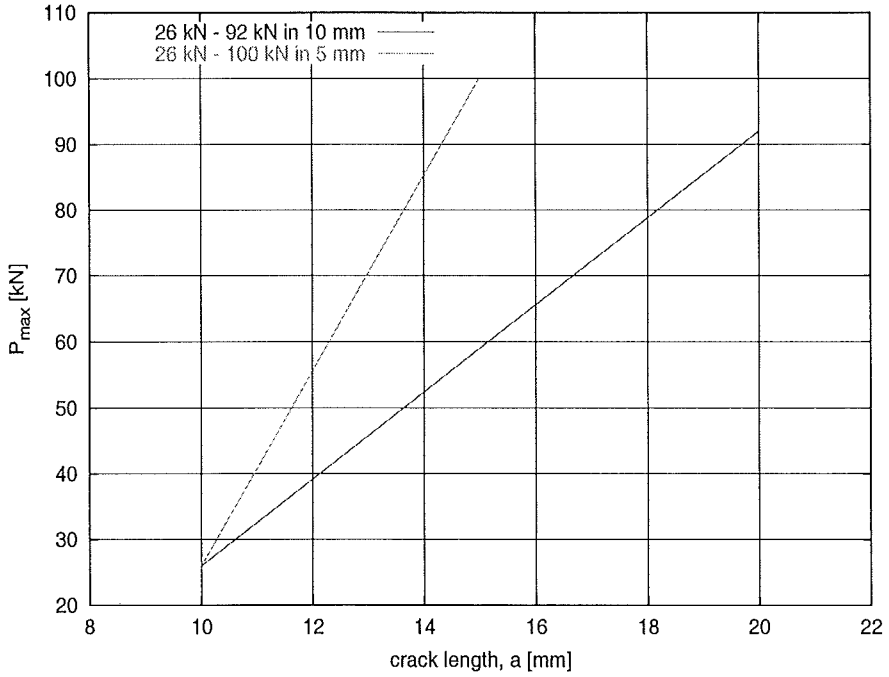

Figure 3.8: Load history of the increasing amplitude tests.

Increasing Amplitude Tests in Lab Air

Since the increasing amplitude (IA) load would be used in the seawater test, a validation of the method was necessary. The first validation was conducted in lab air, with R = 0.1 and a frequency of 10 Hz. There were two tests in the validation: IA in 5 mm crack length and IA in 10 mm crack length. The load history of two cases are presented in Figure 3.8. The pre-cracking load prior to IA test and the load history after IA test are not included in the figure. They can be found in Appendix A5. These load histories resulted in a ΔK range from 6 MPa$\sqrt{}$m to 24 MPa$\sqrt{}$m in only 5 mm crack length, and a ΔK range from 6 MPa$\sqrt{}$m to 26 MPa$\sqrt{}$m in 10 mm crack length.

Another IA test was also conducted with an irregular step-wise load. This test was intended to investigate whether the non-linear IA load affected the crack growth or not. The test was carried out at a frequency of 10 Hz and R = 0.1. The load increment at every step was about 5% of the previous step. The load history of the step-wise IA test is illustrated in Figure 3.9.

Increasing Amplitude Tests in Seawater

The next step of the experiment was to validate the increasing amplitude test in seawater. The first test was conducted by using step-wise increasing load at a frequency of 10 Hz and R = 0.1. The load increment in every step was about 10% of the previous step. The load history of the IA test is presented in Figure 3.10. As a reference, a CA test was also carried out at a frequency of 10 Hz and R = 0.1.

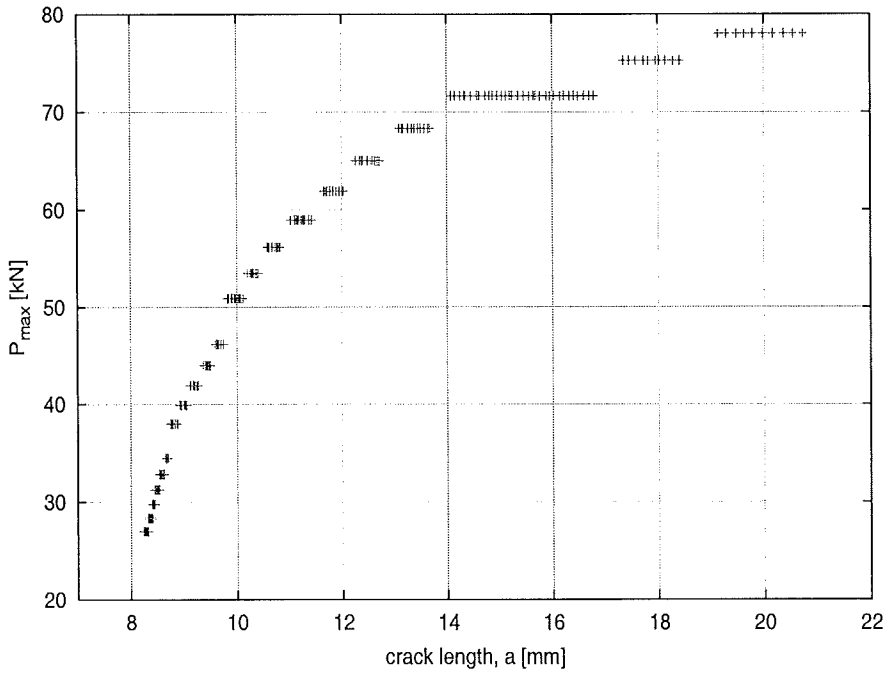

Figure 3.9: Load history of the irregular step wise IA test at a frequency of 10 Hz and R = 0.1 in lab air.

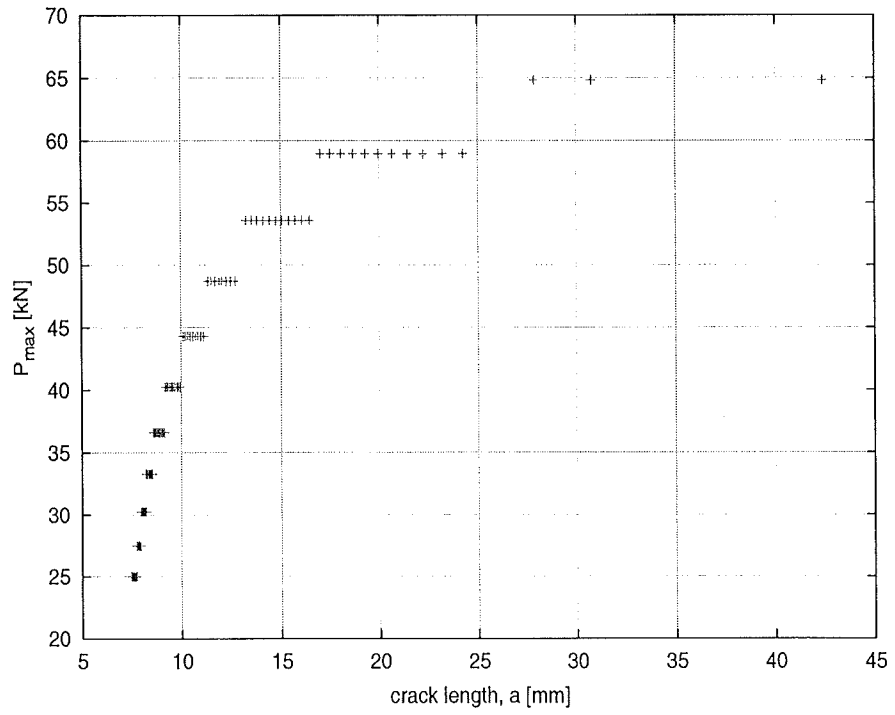

Figure 3.10: Load history of IA test in seawater at a frequency of 10 Hz and R = 0.1.

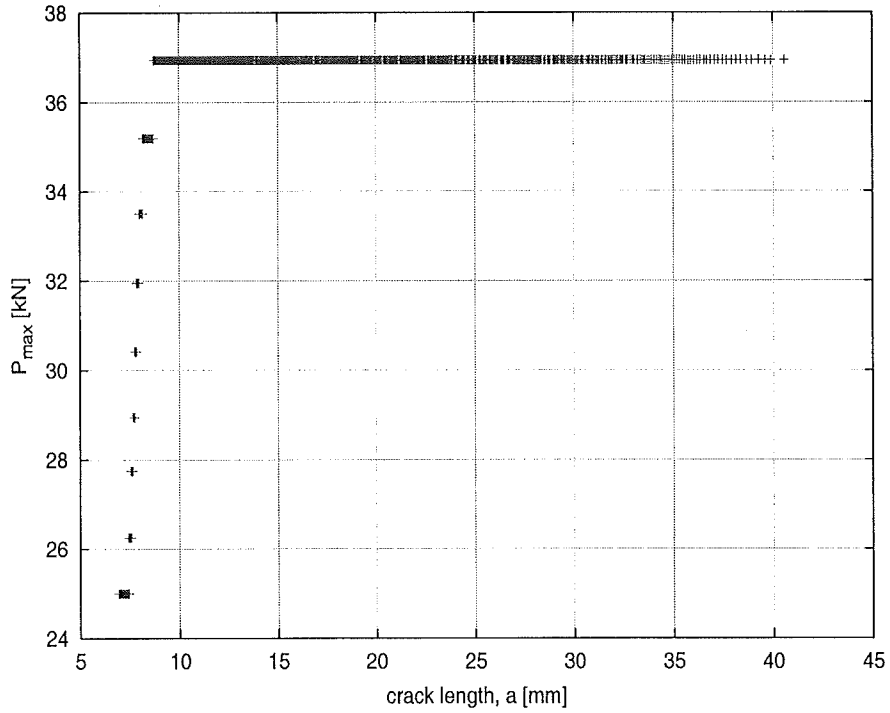

Figure 3.11: Load history of the stepwise followed by a CA test at a frequency of 1 Hz and R = 0.1.

The second test was conducted at a frequency of 1 Hz and R = 0.1. There were four types of loading for the second test: combination of step-wise IA followed by CA, step-wise IA, linear IA, and CA load as a reference. The linear IA and CA tests were carried out twice. The first loading type can be seen in Figure 3.11, the load increment of the step-wise part was 5% of the previous step, and the length of every step was about 0.1 mm. The CA part started at a = 8.7 mm until failure with P_{max} = 37 kN ($\Delta K \approx$ 6.8 MPa$\sqrt{\text{m}}$). The second loading type, the step-wise IA, was applied to investigate whether the transition effect as explained in Sub-section 2.1.3 would significantly affect the results or not. The load increment in the step-wise IA test was 6% of the previous step, and the length of every step was 0.3 mm (see Figure 3.12). The third type was the linear IA with P_{max} increased from 32 kN until 80 kN in 10 mm (from a = 7 mm to a = 17 mm, see Figure 3.13).

The third test was also carried out with a linear IA load at a frequency of 1 Hz but with R = 0.5. It was expected that with such a stress ratio the closure effect and the transition effect could be eliminated. The load history of the test is presented in Figure 3.14. Two CA tests at the same frequency and stress ratio were also carried out as a reference.

3.7.4 Effects of Load Frequency

The objective of the tests was to investigate the effects of the load frequency on the fatigue crack growth rate.

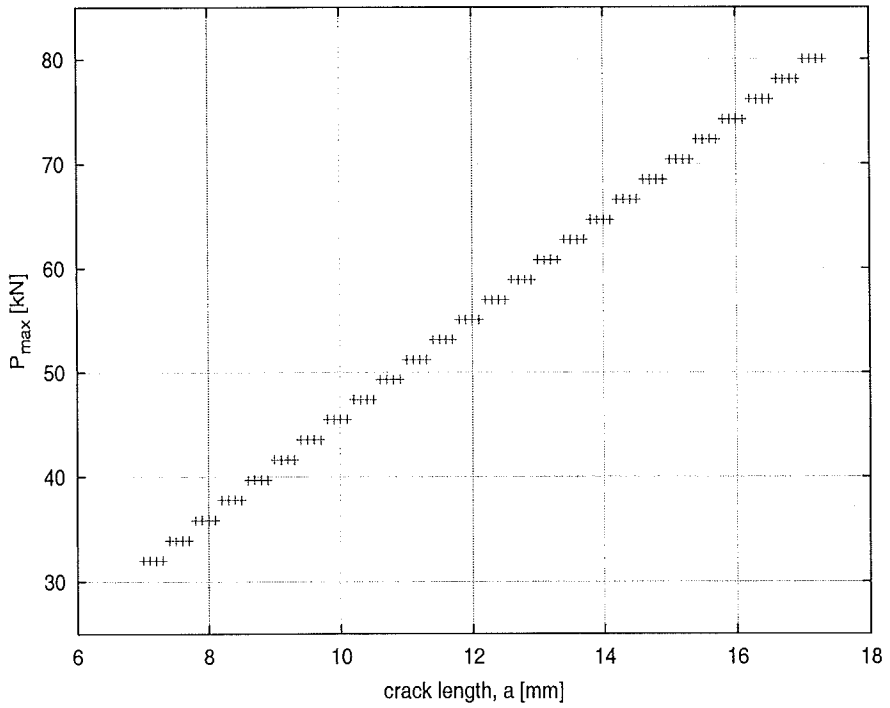

Figure 3.12: Load history of the step-wise IA test at a frequency of 1 Hz and R = 0.1.

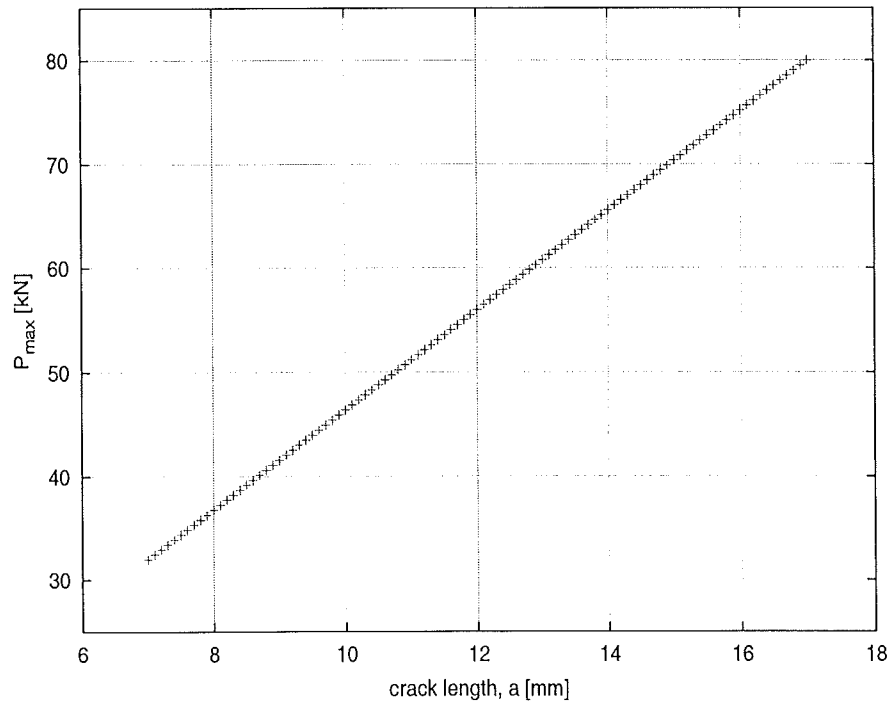

Figure 3.13: Load history of the linear IA test at a frequency of 1 Hz and R = 0.1.

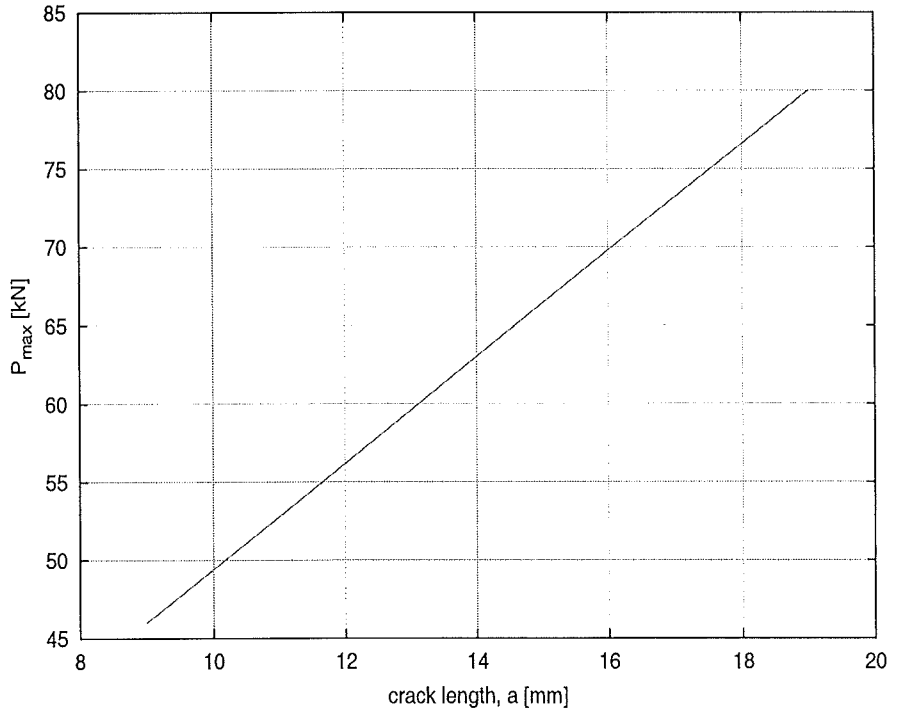

Figure 3.14: Load history of the linear IA test at a frequency of 1 Hz and R = 0.5.

Load Frequency Effects in Lab Air

In order to check whether there was a frequency effect in lab air or not, a test was conducted by alternating the loading frequency between 10 Hz and 0.1 Hz. The load amplitude was kept constant (constant amplitude test). The complete schedule of the test is given in Table 3.3.

Tests at Various Load Frequencies in Seawater

There were two tests which carried out with IA load in order to save the time. The first test was conducted at a frequency of 10 Hz and the second test was at 1 Hz. The stress ratio of both tests was 0.1. Actually, the tests has been explained in the previous sections and they can be compared

Table 3.3: Load frequency versus crack length.

crack length [mm]	load frequency [Hz]
6 - 13	10
13 - 17	0.1
17 - 27	10
27 - 35	0.1
35 - 42	10

based on the load frequencies. Both the 10 Hz and 1 Hz tests are taken from Section 3.7.3 and the load histories are illustrated in Figure 3.10 and 3.13 respectively.

Chapter 4

Results

The results of the experiments that are explained in Section 3.7 are presented in the following sections.

4.1 Preliminary Testing

4.1.1 Validation of Calibration for MTS Machine

The comparison of the crack growth curves between MTS and SCHENCK machines can be seen in Figure 4.1.

4.1.2 Validation of Calibration in Seawater

The comparison of the crack growth curves between visual and Howden measurements is presented in Figure 4.2.

4.1.3 Investigation of The Use of Fresh/Unfresh Seawater

The crack growth curves of tests in fresh and unfresh seawater are presented in Figure 4.3.

4.1.4 Investigation of The Use of Anaerated/Aerated Seawater

The crack growth curves of tests in anaerated and aerated seawater are presented in Figure 4.4.

4.2 Effects of Stress Ratio

4.2.1 Tests at Various Stress Ratios in Lab Air

The crack growth curves at various stress ratios in lab air are presented in Figure 4.5.

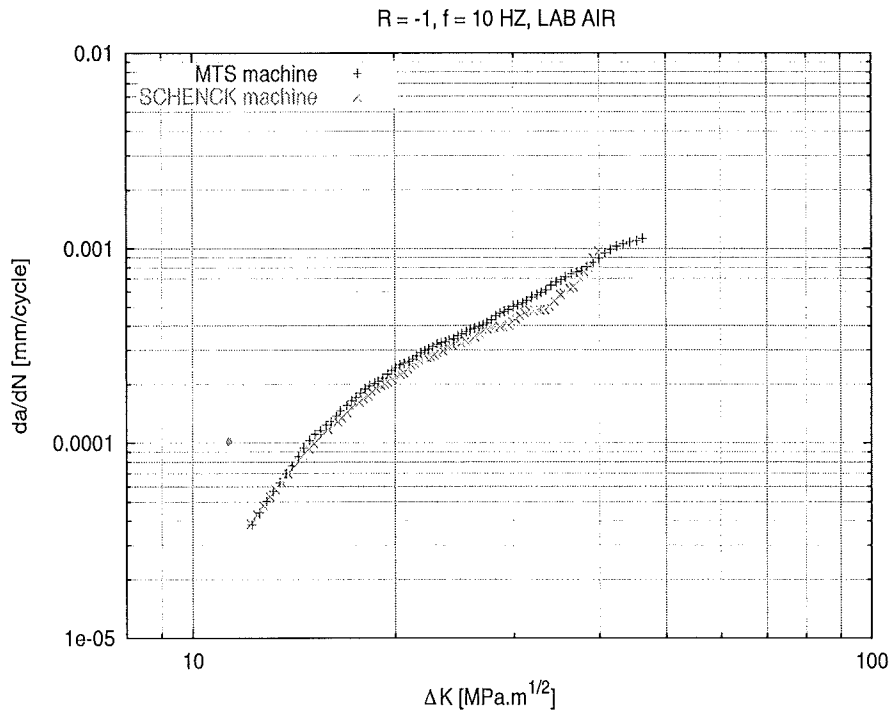

Figure 4.1: Comparison of the crack growth curves from SCHENCK and MTS machines.

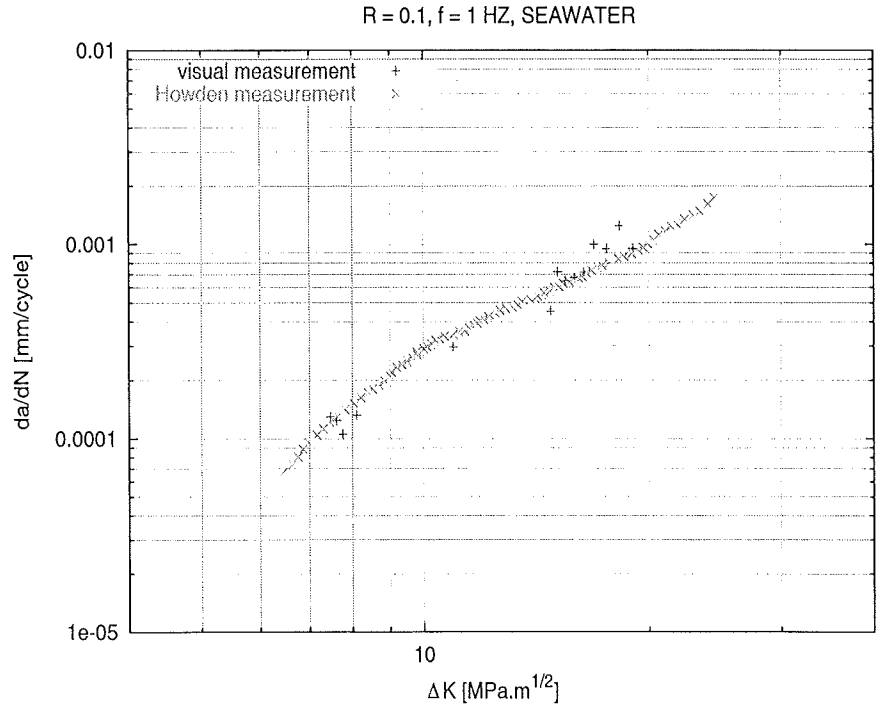

Figure 4.2: Comparison of da/dN vs ΔK curves between visual and Howden measurements in seawater.

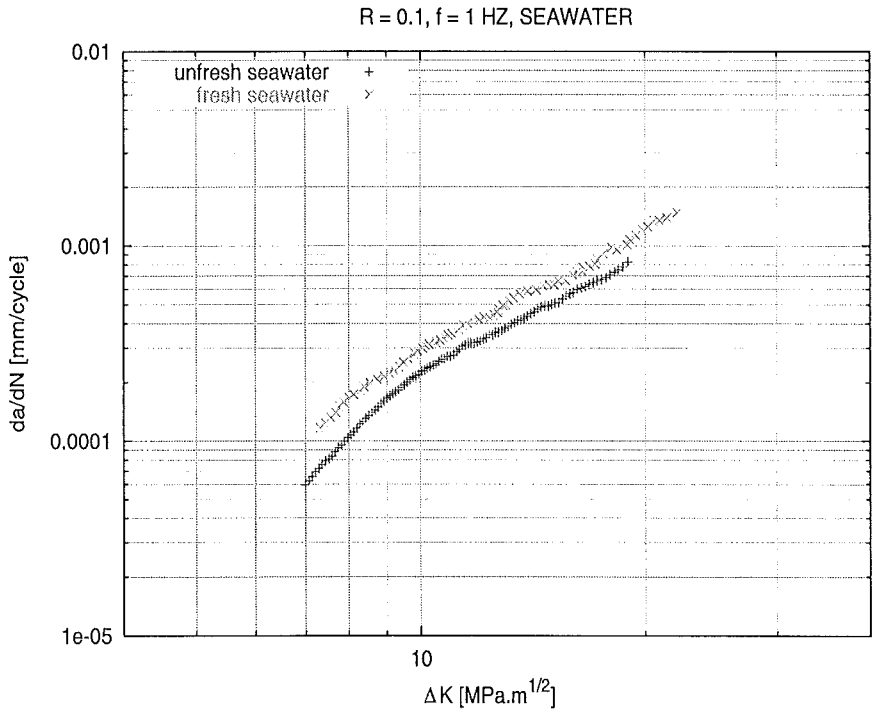

Figure 4.3: Crack growth curves in fresh and unfresh seawater.

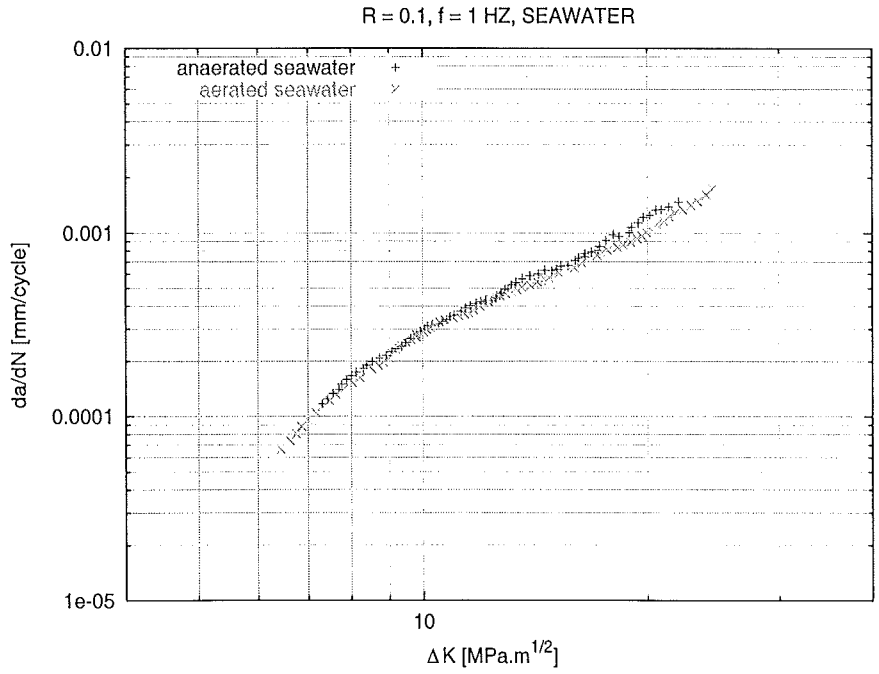

Figure 4.4: Crack growth curves in anaerated/aerated seawater condition.

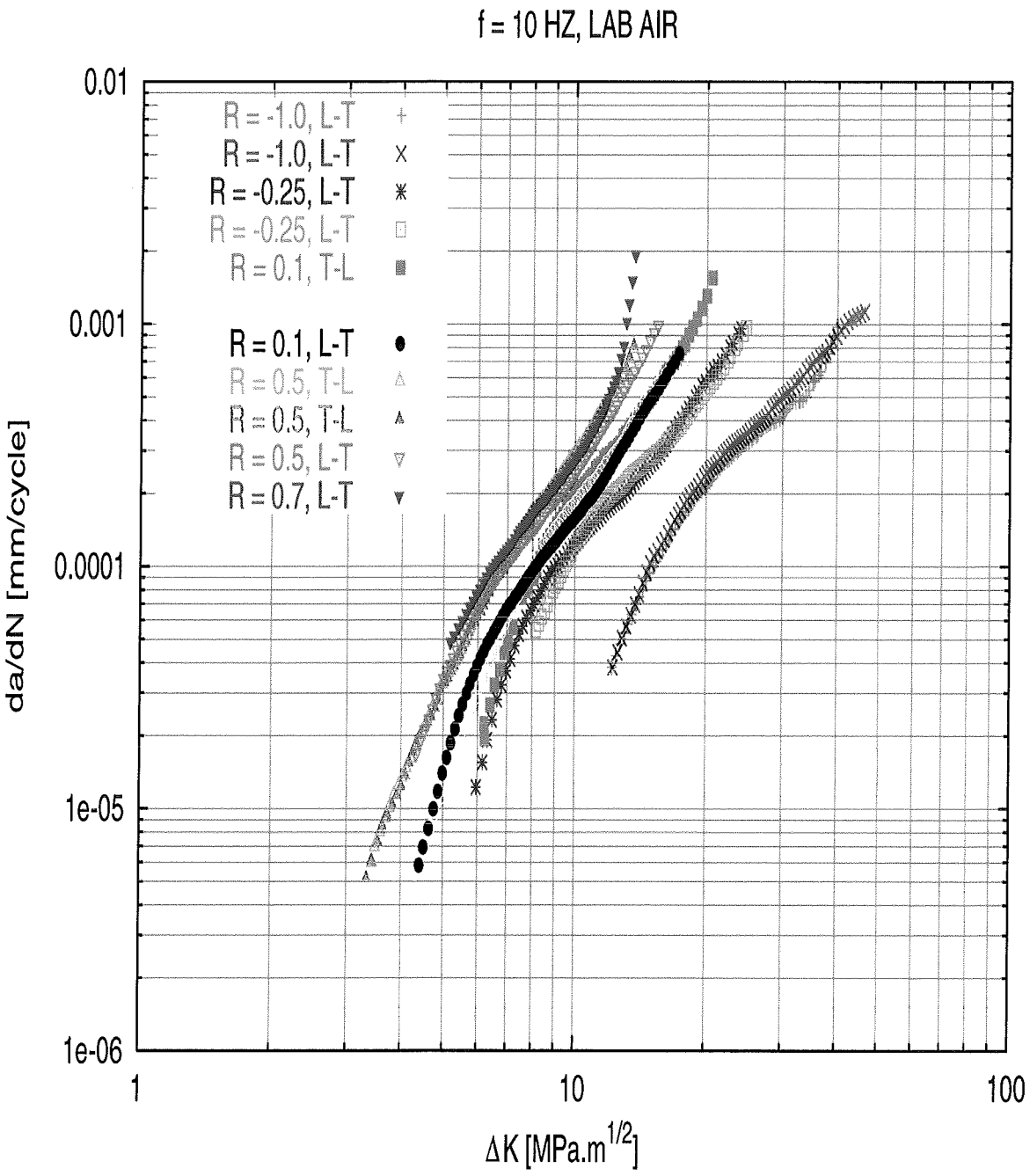

Figure 4.5: Crack growth curves of AA 5083-H321 at various stress ratios.

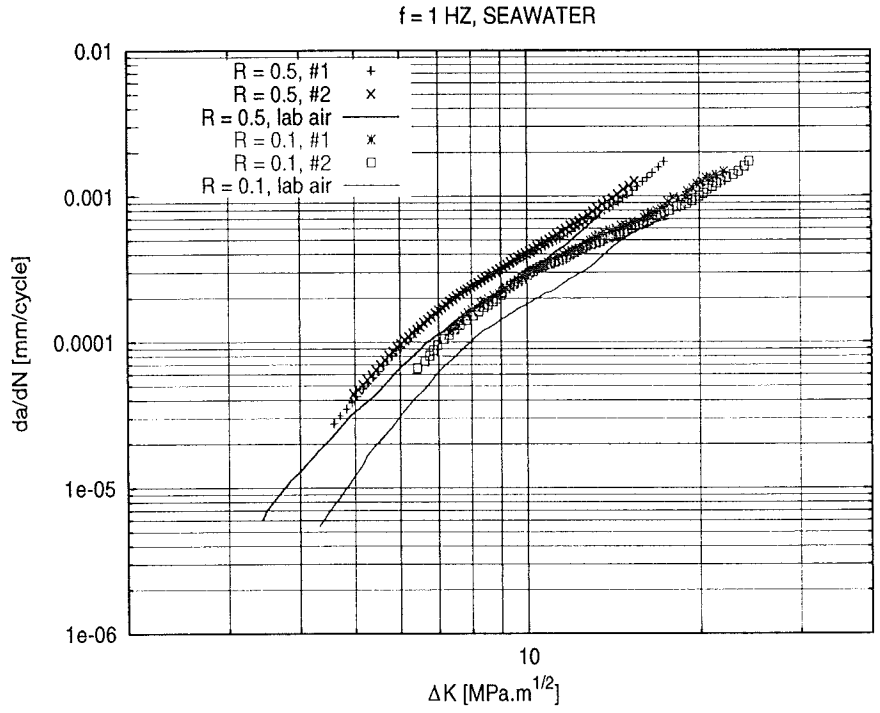

Figure 4.6: Crack growth curves at different stress ratios in seawater.

4.2.2 Tests at Various Stress Ratios in Seawater

The results of tests at stress ratios of 0.1 and 0.5 in seawater are presented in Figure 4.6. Results in lab air are also presented as a reference.

4.3 Increasing Amplitude (IA) Tests

4.3.1 Increasing Amplitude (IA) Tests in Lab Air

The crack growth curves of the linear IA tests are presented in Figure 4.7. A crack growth curve of CA test is also presented as a reference.

The crack growth curves of the step-wise IA test is presented in Figure 4.8. A CA test and a linear IA test (IA in 10 mm) with the same frequency and stress ratio are also given as a reference.

4.3.2 Increasing Amplitude (IA) Tests in Seawater

The crack growth curves of the step-wise IA and CA tests at a frequency of 10 Hz and R = 0.1 can be seen in Figure 4.9.

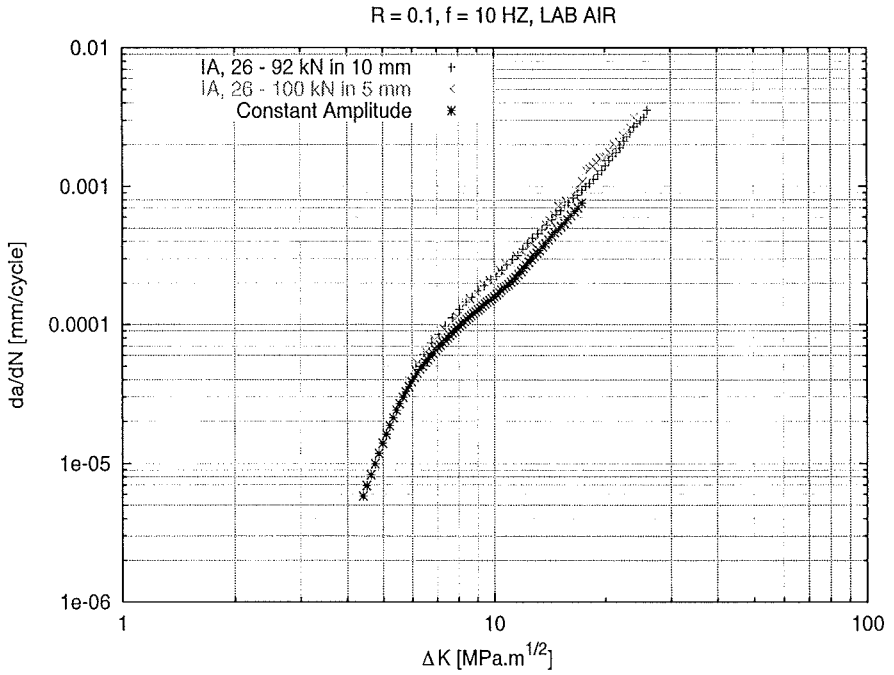

Figure 4.7: Crack growth curves of the IA and the CA tests.

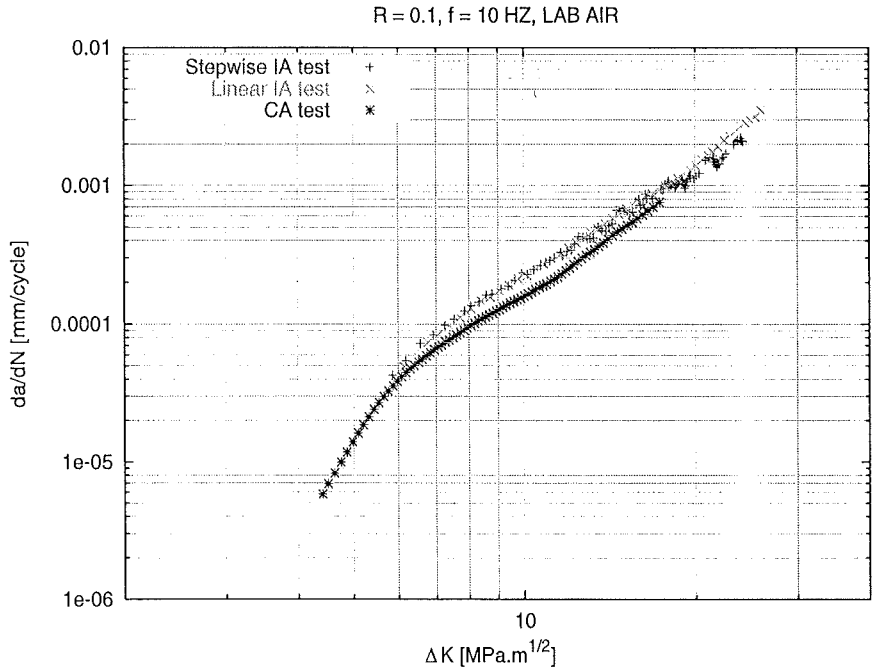

Figure 4.8: Crack growth curves of the step-wise IA and the CA tests.

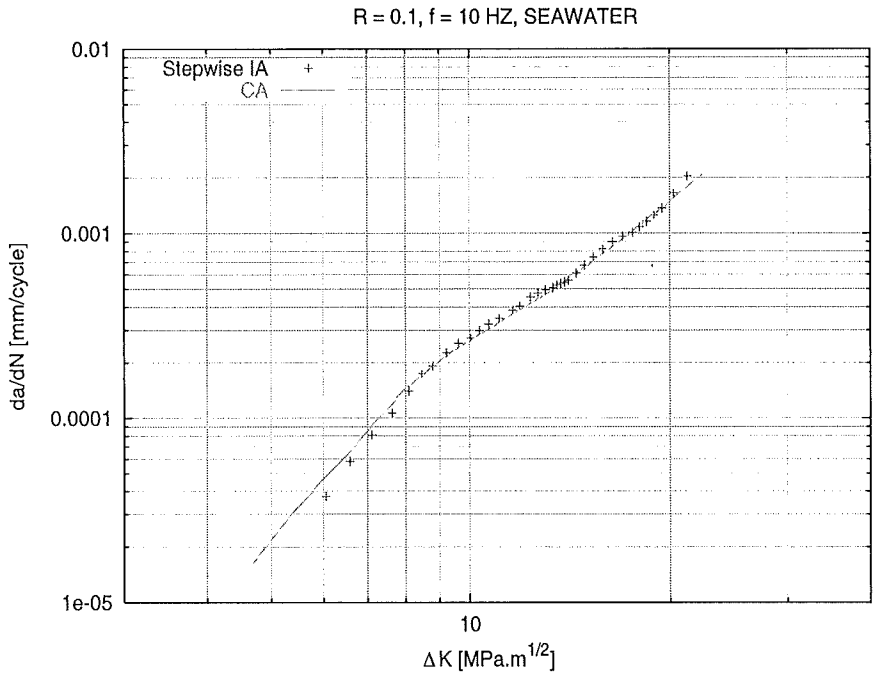

Figure 4.9: Crack growth curve of the step-wise IA test at f = 10 Hz and R = 0.1.

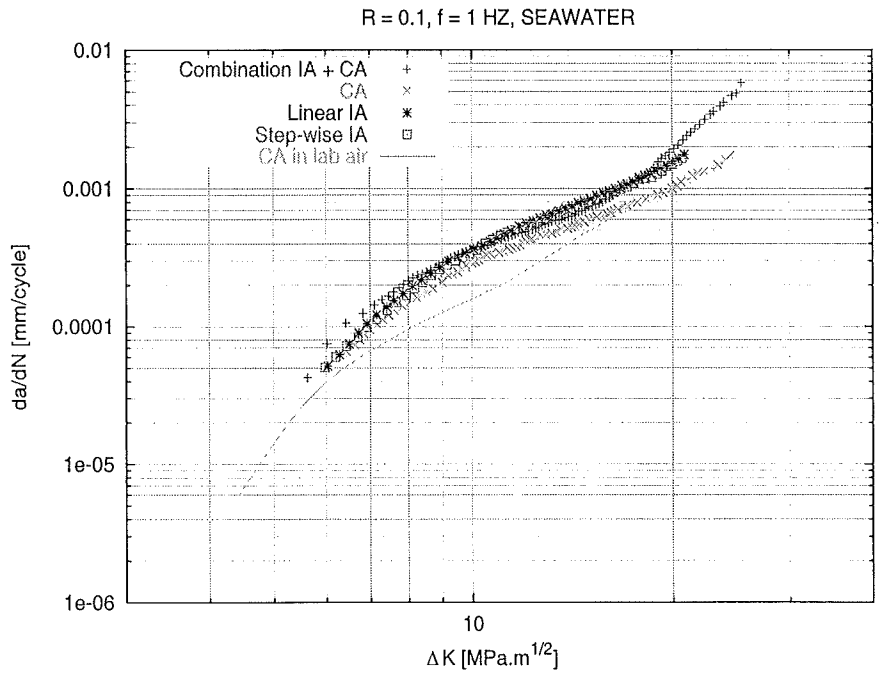

Figure 4.10: Crack growth curves of IA tests at f = 1 Hz and R = 0.1. A result of a test in lab air is also presented as a reference.

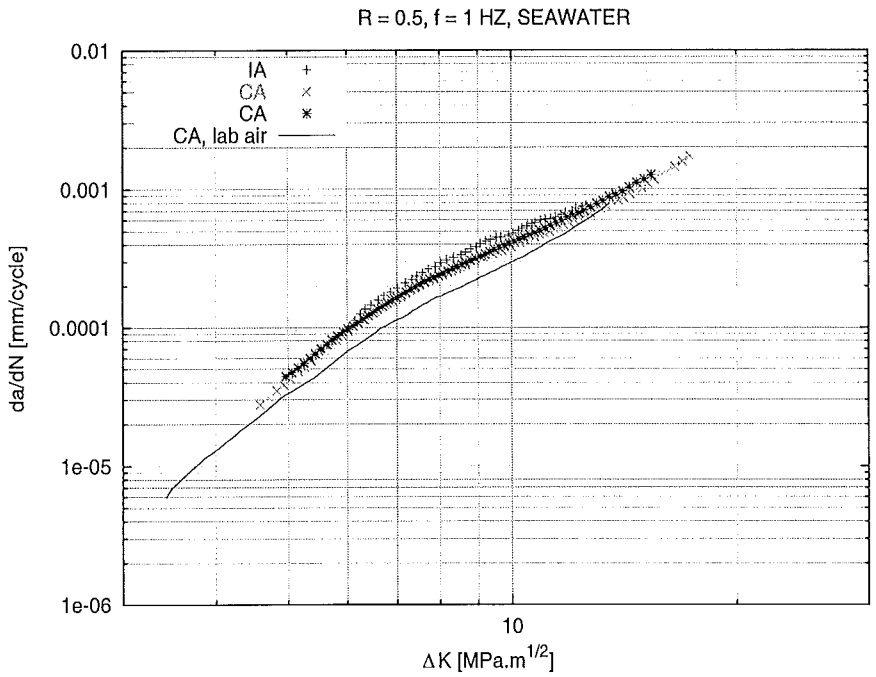

Figure 4.11: Crack growth curves of IA test and CA tests at a frequency of 1 Hz and R = 0.5.

The crack growth curves of combination IA+CA, step-wise IA, linear IA, and CA tests are presented in Figure 4.10. For the sake of clarity, only one crack growth curve from every load type is presented because the other results are similar.

The crack growth curves of the IA test at a frequency of 1 Hz and R = 0.5 is presented in Figure 4.11. The results from the CA tests at the same frequency and stress ratio are also presented as a comparison.

4.4 Effects of Load Frequency

4.4.1 Load Frequency Effects in Lab Air

The crack growth curve with the alternating load frequency of 10 Hz and 0.1 Hz is described in Figure 4.12. A crack growth curve of CA test is also presented as a reference.

4.4.2 Tests at Various Load Frequencies in Seawater

The crack growth curves of tests at frequencies of 1 Hz and 10 Hz are presented in Figure 4.13 along with the crack growth curve in lab air as a reference.

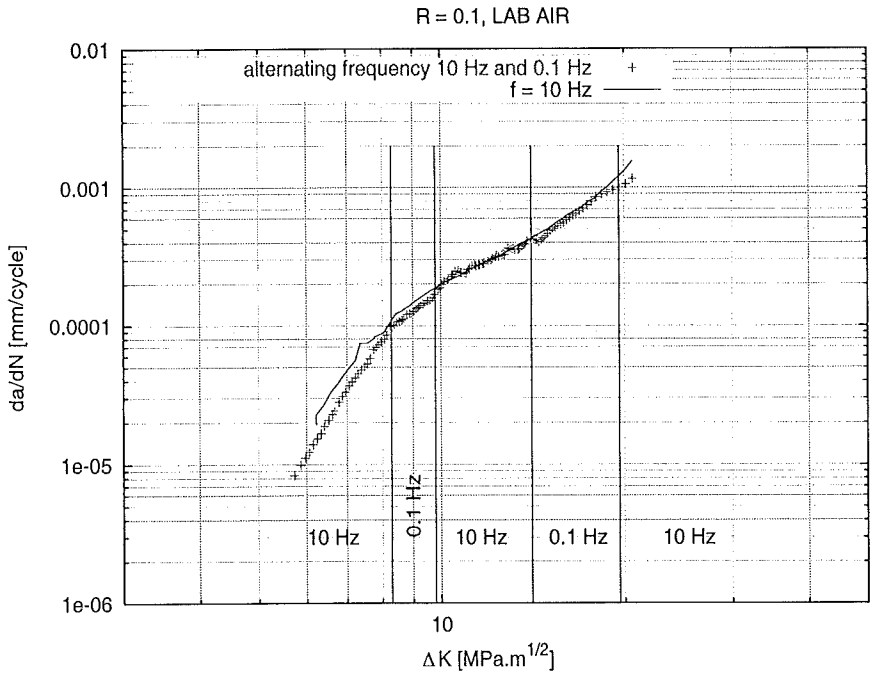

Figure 4.12: A crack growth curve of the alternated load frequency test.

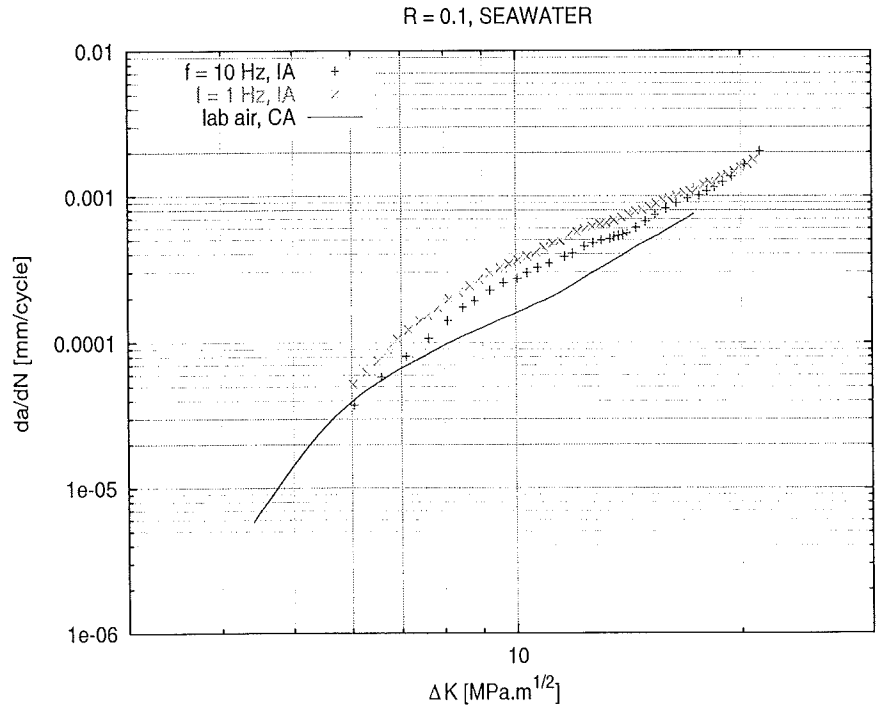

Figure 4.13: Crack growth curves at frequencies of 1 Hz and 10 Hz in seawater.

Chapter 5

Discussion and Analysis

Based on the results presented in the previous chapter, every test is discussed and analysed in the following sections.

5.1 Preliminary Testing

5.1.1 Validation of Calibration for MTS Machine

From Figure 4.1 it can be seen that the calibration curve for the SCHENCK machine can also be used for the MTS machine. There is no significant difference between the two results although the controlling equipment of both machines is different.

5.1.2 Validation of Calibration in Seawater

Figure 4.2 shows that the calibration curve in lab air still can be used in seawater environment. The scatter of the visual measurement is most probably due to the error of the crack length reading. By comparing the crack growth curves, the crack length measurement of both methods as well as the electric potential effect on the crack growth rate can be observed. Obviously, there is no effect of the seawater on the Howden measurement. Furthermore, the corrosion fatigue crack growth mechanism is also not affected by the applied electrical potential from the Howden equipment. This is theoretically expected because the conductivity of aluminum alloy is far higher than that of the seawater (metal conductivities are between 10^5 - 10^6 $[\Omega^{-1}\text{cm}^{-1}]$ compared to aqueous conductivities of 10^{-6} - 10^{-1} $[\Omega^{-1}\text{cm}^{-1}]$ [17]), hence only a very low electric current is transmitted via the seawater.

5.1.3 Investigation of The Use of Fresh/Unfresh Seawater

A comparison of two crack growth curves (the fresh and unfresh seawater) can be found in Figure 4.3. Obviously, the test in unfresh seawater results in a lower crack growth rate than in fresh seawater. This is most probably due to the lack of oxygen supply in the seawater since

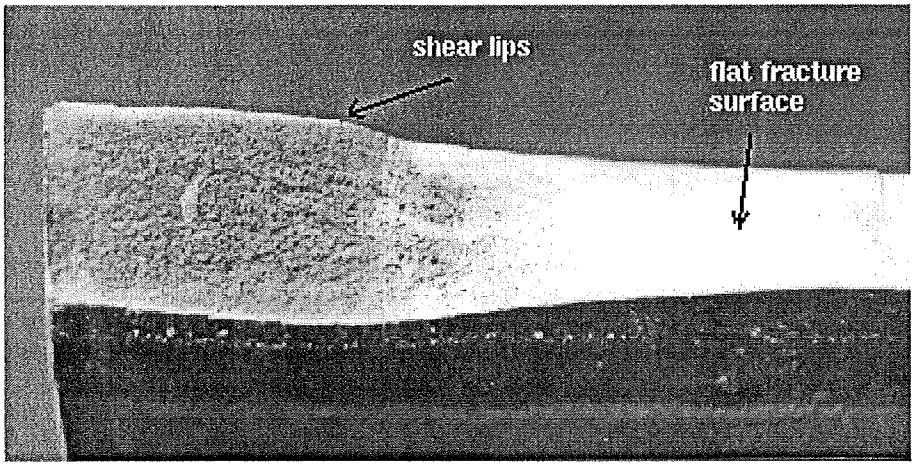

Figure 5.1: Flat and slant fracture surfaces.

anaerated seawater was used. Theoretically, in the fresh seawater the oxygen concentration is high but after a certain period of time the concentration drops because it has been used in the corrosion process. Natural oxygen diffusion takes a long time, therefore needs to be applied artificially.

5.1.4 Investigation of The Use of Anaerated/Aerated Seawater

From Figure 4.4 it can be concluded that there is no significant difference in the crack growth curves between aerated and anaerated seawater. Both tests took three days to finish. It seems that the anaerated seawater still has enough oxygen to supply the corrosion process for three days. However, to simulate natural seawater, the aerated seawater was used in the corrosion fatigue crack growth test. The reason is that waves and streams in sea ease the solubility of oxygen in seawater. It was decided that the seawater was replaced after one week of testing as recommended by ASTM E647 [15].

5.2 Effects of Stress Ratio

5.2.1 Tests at Various Stress Ratios in Lab Air

Figure 4.5 shows that there is no significant difference in crack growth behavior between T-L and L-T specimens. Only at the beginning of the curves shows a significant difference. This is most probably due to the different initial condition of the notch which can give a different state of stress. Moreover, the loading history from the precracking stage, which occurs prior to the tests can also cause this difference. There is a possibility that a small overload/underload can occur at the initial loading due to the lack of control of the testing machine.

From Figure 4.5 it can be noticed that all crack growth curves shows a change of the slope at $da/dN \approx 10^{-4}$ mm/cycle. This value is also observed for other aluminum alloys such as 2024 - T3 [18]. An observation on the fracture surface reveals that this can be attributed to the formation of shear lips. At $da/dN < 10^{-4}$ mm/cycle the fracture surface is flat, and at $da/dN \approx 10^{-4}$ mm/cycle the shear lips start to grow (see Figure 5.1) resulting in a slant fracture surface. In static fracture mechanics, the formation of the shear lips is due to the relative dimension of the crack tip plastic zone and the plate thickness [2]. However, under cyclic loading the process is more complicated, and the mechanisms responsible for the transition from flat surface to slant surface are still ambiguous.

It can also be noticed from Figure 4.5 that all curves have the similar shape, they only shift to the left as the stress ratio increases. In other words, the crack growth rate increases with increasing of the stress ratio at the same ΔK level. This is theoretically expected, because the crack closure effects are smaller at higher stress ratios and lead to a higher da/dN. At high stress ratios such as R = 0.5 and R = 0.7, the crack closure has no effects at all, since the crack mouth is widely open all the time. This is demonstrated in Figure 4.5 where the crack growth curve of R = 0.7 corresponds to that of R = 0.5. A consequence of these findings is that if the effect of the crack closure can be formulated, Figure 4.5 can be presented in only one curve as explained in Subsection 2.1.2. By assuming that the same da/dN is resulted from the same ΔK_{eff}, a crack closure formulation is proposed as in Equation 5.1.

$$U = 0.02R^2 + 0.32R + 0.66 \tag{5.1}$$

and,

$$\Delta K_{eff} = U.\Delta K \tag{5.2}$$

By applying equation 5.1 and 5.2, Figure 4.5 can be presented as da/dN vs ΔK_{eff} instead of da/dN vs ΔK as seen in Figure 5.2.

5.2.2 Tests at Various Stress Ratios in Seawater

Results of tests at various stress ratios in seawater as seen in Figure 4.6 show that the crack growth curves of lab air and seawater are still comparable. The shape of the curves are similar, the curves only shift upward in seawater environment. In other words, the formation of the shear lips is delayed in seawater (about 2 x 10^{-4} mm/cycle compared to 10^{-4} mm/cycle in lab air). However, these findings are still not understood because the formation mechanism of the shear lips under cyclic load is not clear. Another interesting finding is that apparently the closure formulation in seawater is the same as that in lab air. This can be proved by applying the closure formulation (Equation 5.1) to the crack growth curves in seawater as illustrated in Figure 5.3. Crack growth curves in lab air are also presented as a reference. As a consequence of this finding is that σ_{op}/σ_{max} in seawater is the same with that in lab air because U (closure formulation) is the same. This can be explained by Equation 5.3 and 5.4.

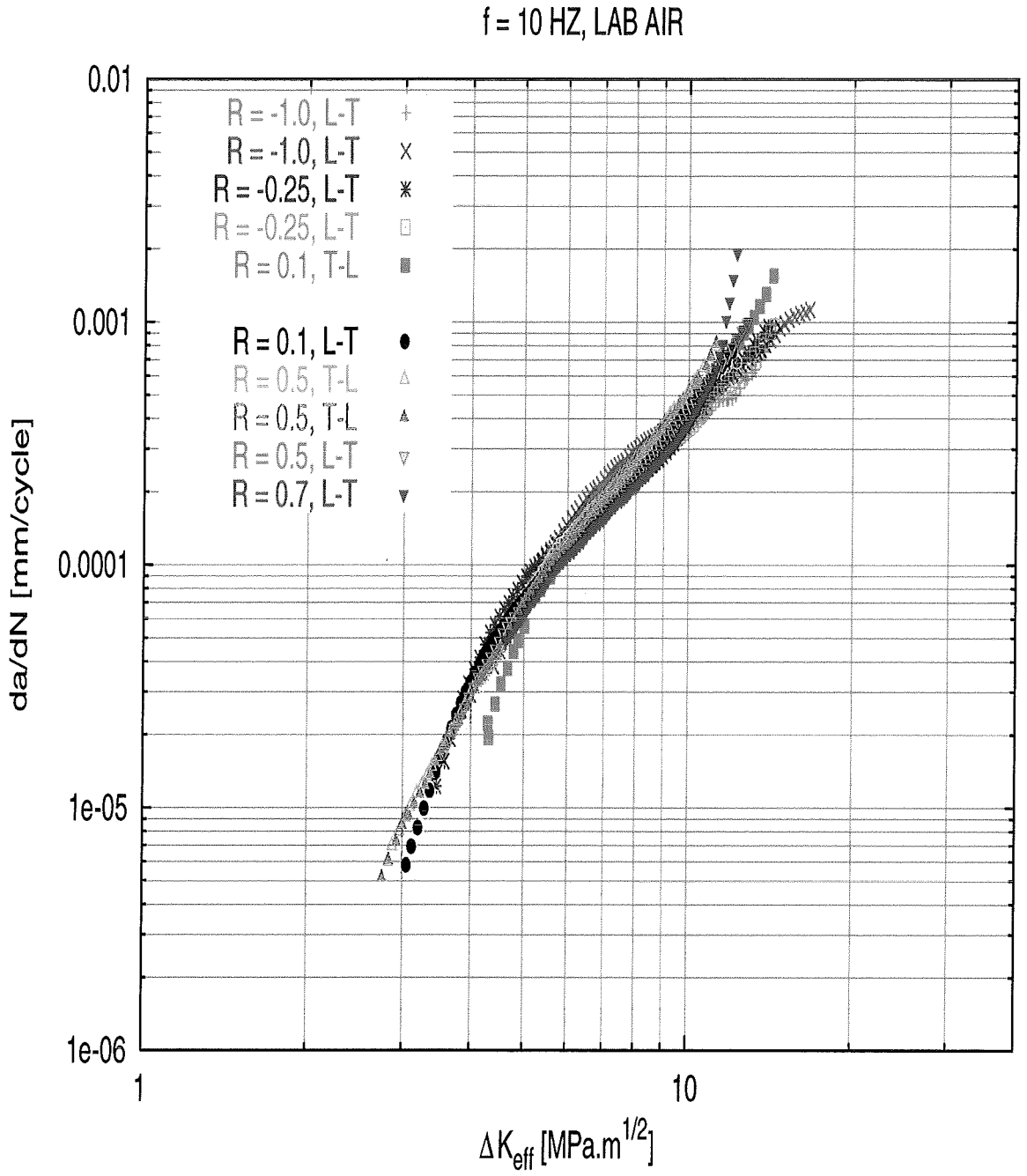

Figure 5.2: da/dN vs ΔK_{eff} curves at various stress ratios in lab air.

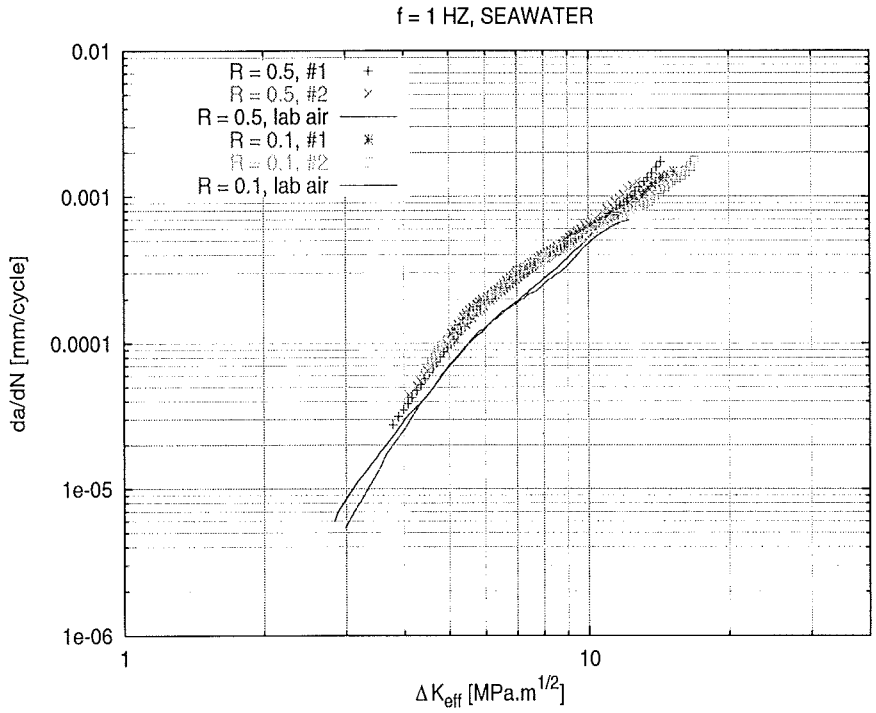

Figure 5.3: Graphics of da/dN vs ΔK_{eff} of the crack growth in seawater.

$$U = \frac{\Delta K_{eff}}{\Delta K} = \frac{\sigma_{max} - \sigma_{op}}{\sigma_{max} - \sigma_{min}} = \frac{1 - \sigma_{op}/\sigma_{max}}{1 - R} \tag{5.3}$$

or,

$$\sigma_{op}/\sigma_{max} = 1 - U(1 - R) \tag{5.4}$$

It can also be noticed from Figure 4.6 and 5.3 that at higher ΔK levels the crack growth rate in seawater is the same with that in lab air. Obviously, at higher ΔK levels the mechanical factor is dominant compared to that of the environment. At such ΔK levels, the contribution of the mechanical factor to the crack growth rate is more than that of the environment. There might be a threshold value of the contribution to the crack enhancement by the environment. This finding is also observed by other researchers [19]. Figure 4.6 also reveals that at higher stress ratios, the environment effect is not prominent. This is indicated by the crack growth curve at low ΔK levels, which shows no differences between the crack growth rate in lab air and in seawater. It seems that seawater affects mostly on the reduction of the closure effect, only small contribution to the crack enhancement. This is illustrated by Figure 5.3 where the closure effect is eliminated by using ΔK_{eff} instead of ΔK. Obviously, the effect of seawater on the crack growth rate at a frequency of 1 Hz is small in this alloy.

5.3 Increasing Amplitude (IA) Tests

5.3.1 Increasing Amplitude Tests in Lab Air

Observations of the results of both IA tests (in 5 mm and 10 mm crack length) show that there is no significant difference between the crack growth curves of IA tests and that of the CA test (see Figure 4.7). However, if the results are observed carefully, the IA crack growth are slightly higher than that of CA crack growth. This is most probably due to the transition effect as explained in Section 2.1.3. In IA test the load as illustrated in Figure 2.4(b) is applied consecutively and results in a higher ΔK_{eff} during the test. This is because the opening stress (σ_{op}) has no enough time to return to the normal level. Another possibility is due to the less effect of the shear lips on the IA tests compared to the CA test, since the IA tests were carried out in shorter crack lengths (5 mm and 10 mm) than those in the CA test (> 30 mm). However, the last possibility does not seem dominant because the crack growth curves for crack length 5 mm and 10 mm are similar. If the shear lips have large effects on the crack growth rate, both IA tests should be slightly different. The second test also shows the same tendency (see Figure 4.8) although the step-wise IA load was applied. It is expected that such a load can give enough time for σ_{op} to return to the normal level. However, the step is not long enough to reduce the transition effect. It seems that the shear lips effects are not dominant factors that cause the difference, because the final crack lengths are the same as the CA test. If such effects are prominent the crack growth curve should be similar to that of the CA test.

Another problem encountered in the IA tests is that the actual load is quite different than the expected load. A comparison between the expected load and the measured load is illustrated in Figure 5.4. Only P_{max} presented in the figure because the load fluctuation is greater than that in P_{min}. The fluctuation in the actual load is due to the fluctuation in the crack length measurement, since the load amplitude depends on the measured crack length ($P = f(a)$). However, the fluctuation is not significant and the overall load curve still follows the expected load.

5.3.2 Increasing Amplitude Tests in Seawater

The crack growth curve of the IA test at a frequency of 10 Hz and R = 0.1 shows good agreement with that of the CA test as seen in Figure 4.9. Surprisingly, the step-wise IA load does not cause a higher crack growth rate which occurs under the step-wise IA load in lab air. It seems that σ_{op} is not affected by the step-wise IA load. There might be corrosion product on the crack surface which, in such a way, results in the same closure effect as in the CA test.

The second test is intended to confirm the previous test with a loading frequency of 1 Hz and R = 0.1. Results of the combination IA+CA, step-wise IA and linear IA show a good agreement as seen in Figure 4.10. Obviously, the same closure effect occurs in these three types of loading. However, unlike the previous test these results are slightly higher than those of the CA test. The lower frequency may have caused a different closure effect compared to the previous test.

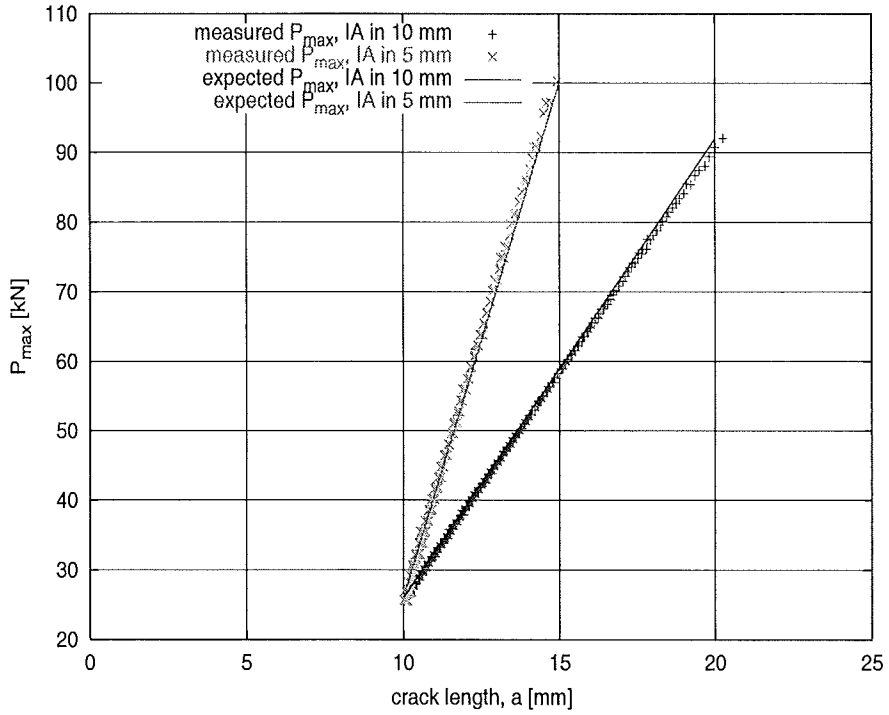

Figure 5.4: Comparison between the measured and the expected load.

The combination of IA+CA loads results in a higher crack growth rate compared to the CA load, although the IA part is only from a = 6 mm until a = 8.7 mm. Apparently, the shear lips and the transition effects are not relevant because the final crack length is the same as that of the CA load, and the IA load is only applied at a quite short crack length. Another possibility is that corrosion products reduce ΔK_{eff}, because it can cause the wedging effect between the crack surfaces. In the CA test, the deposition of the corrosion product is more than that in IA test because the duration of the test is longer.

It seems that the step-wise IA has no significant effects if it is compared to the linear IA test. However, a further investigation of the measured load history reveals that the step-wise IA is not really applied to the specimen, especially at the crack length longer than 11 mm. The measured load history is illustrated in Figure 5.5 (compare with the expected load presented in Figure 3.12). This might cause the crack growth curve of the step-wise IA is similar to the linear IA curve.

The result of the linear IA test at R = 0.5 (Figure 4.11) shows that there is still a slight increase in the crack growth rate. According to the result at various stress ratios in lab air (Figure 4.5), at R = 0.5 the closure effect as well as the transition effect should be eliminated because $\sigma_{op} = \sigma_{min}$. Thus, the most plausible reason for the increase in crack growth rate is the corrosion product deposits on the crack surfaces. However, a further observation with SEM is needed to verify this assumption or to reveal other reasons.

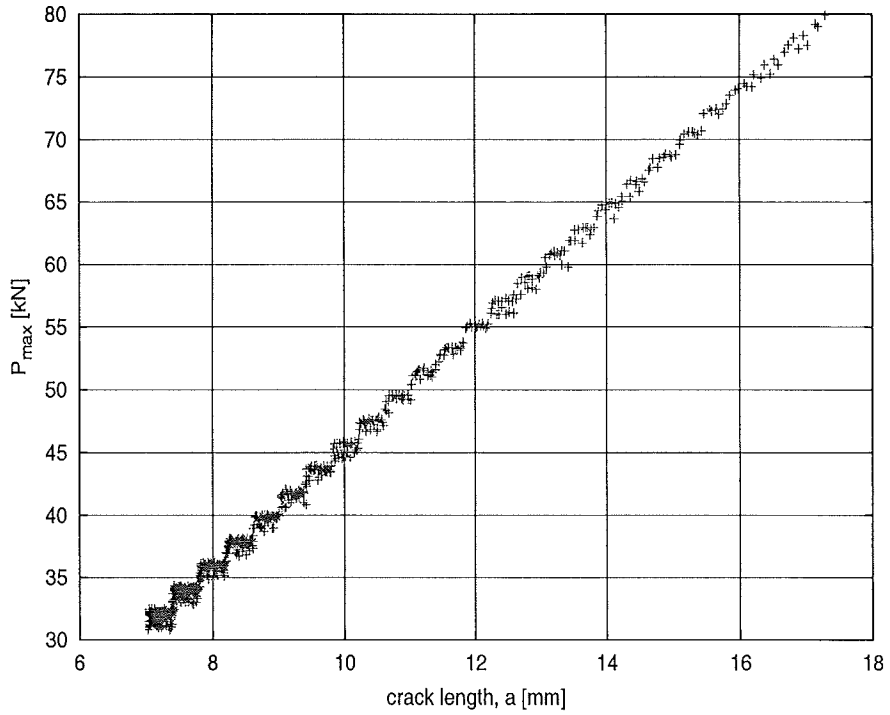

Figure 5.5: A measured load history of the step-wise IA.

5.4 Effects of Load Frequency

5.4.1 Load Frequency Effects in Lab Air

As seen in Figure 4.12, the effect of loading frequency is negligible in lab air. It seems that the oxide layer works well in such an environment. It can be understood because lab air is not an aggressive environment. In other words, fatigue crack growth tests in lab air can be accelerated by applying high load frequencies without obtaining different results. Note that this finding is obtained for aluminum alloy 5083-H321, other materials may have different reactions or responses to such an environment.

5.4.2 Tests at Various Loading Frequencies in Seawater

From Figure 4.13, it is obvious that the test at a lower frequency causes a higher crack growth rate. This is due to the fact the the time for the reaction between the fresh crack surface and the environment in a low frequency is longer than that in a high frequency. Thus, the crack enhancement by the environment is larger, and results in a higher crack growth rate. However, the increase in the crack growth with decreasing load frequency from 10 Hz to 1 Hz is only about 25 %. Furthermore, the increase of the crack growth rate at 1 Hz is not more than twice of that in lab air. It seems that the aluminum alloy 5083-H321 has an excellent corrosion fatigue behavior in seawater. These findings should be confirmed with further investigations at very low

frequencies such as 0.1 Hz or even lower. Unfortunately, there are no publications which deal with both the same subject and the same material that can be used as a comparison. However, a result from other researchers [20] with a different temper designation of aluminum alloy (5083 - H12) in 3.5 % NaCl solution at a load frequency of 0.11 Hz and R = 0.3 also shows only 30 % increase in the crack growth rate compared to that in room air. Obviously, as far as corrosion fatigue crack growth behavior is concerned the aluminum alloy 5083 is feasible for structures in seawater environment.

Chapter 6

Conclusion and Remarks

6.1 Conclusion

Based on the results and the analysis as described in the previous chapters, it can be concluded that:

- The calibration curve in lab air for the electric potential difference technique can also be used in seawater.
- In order to simulate natural seawater and to maintain the reproducibility of the test, aerated seawater must be used and it is recommended to replace the seawater every week.
- There is no significant difference in the fatigue crack growth behavior between T-L specimen and L-T specimen.
- There is a change in the slope of the crack growth curves which occurs at $da/dN \approx 10^{-4}$ mm/cycle in lab air and at $da/dN \approx 2\text{x}10^{-4}$ in seawater. This is associated with the formation of the shear lips.
- The crack growth curves at various stress ratios in lab air and seawater can be presented in one crack growth curve by replacing ΔK with ΔK_{eff}. This is done by applying the closure formulation as expressed by the following equation:

$$\begin{aligned} \Delta K_{eff} &= \Delta K.U \\ U &= 0.02R^2 + 0.32R + 0.66 \end{aligned} \tag{6.1}$$

- The crack closure effect in seawater is the same as that in lab air. In other words, σ_{op}/σ_{max} in seawater is the same with that in lab air.
- The increase in the crack growth rate in the increasing amplitude test is attributed to a combination of the closure effect, the transition effect, and the corrosion product deposits on the crack surfaces. In practice, if the increasing amplitude load occurs it will have a serious implication since the actual crack growth can be higher than the predicted value.

- There is no significant effect of load frequency in lab air. This is due to the formation of a passive oxide layer.
- In seawater, lower load frequencies result in higher crack growth rates, because it allows the crack tip and the seawater to interact during a longer period.
- Generally, aluminum alloy AA 5083-H321 has a lower corrosion fatigue crack growth rate in seawater compared to high strength aluminum alloys such as 2xxx and 7xxx series.

6.2 Remarks

Some observations during the experiments remain unclear. Therefore, some remarks and suggestions are given here:

- In order to monitor the condition of the artificial seawater, a regular monitoring of the electrode potential between aluminum and seawater is needed. This allows us to monitor that the electrochemical condition around the crack is the same for every test.
- The crack closure formulation must be also confirmed with a test at negative stress ratios in seawater in order to find out if σ_{op}/σ_{max} is also the same with that in lab air.
- To confirm that the deposition of the corrosion product in the increasing amplitude test is thicker than that in the constant amplitude test, an observation with SEM is needed.
- A further investigation is needed to find out what are the causes of the discrepancies in the crack growth rate between IA test and CA test in lab air as well as in seawater.
- There might be an influence from the temperature variation to the crack growth rates since the seawater temparature is ranging from 21 - 24 ^{0}C. A further investigation of such an effect may be needed, since an increase in the temperature can cause an increase in the crack growth rate. However, the effect is not significant at higher ΔK levels [21].

Bibliography

[1] Hascaryantono, A.P.: *Corrosion Fatigue Crack Growth in Aluminum Alloys*, A Literature Review, Materials Science and Engineering, Delft University of Technology, 2000.

[2] Janssen, M., Zuidema, J., Wanhill, R.J.H.: *Fracture Mechanics*, a provisional edition, TU Delft, The Netherlands, 2000.

[3] Zuidema, J., van Soest, T., Janssen, M.: **Synergetic Effects of Fatigue Crack Closure Mechanisms**, *Advances in Fatigue Crack Closure Measurement and Analysis: Second Volume, ASTM STP 1343*, R.C. McClung and J.C. Newman, Jr., Eds., ASTM, West Conshohocken, PA, 1999, pp. 379 - 389.

[4] Ewalds, H.L., van Doorn, F.C., and Sloof, W.G.: **Influence of Environment and Specimen Thickness on Fatigue Crack Growth Data Correlation by Means of Elber-Type Equations**, *Corrosion Fatigue: Mechanics, Metallurgy, Electrochemistry, and Engineering, ASTM STP 801*, T.W. Crooker and B.N. Leis, Eds., ASTM, 1983, pp. 115 - 134.

[5] Schijve, J.: *Four Lectures on Fatigue Crack Growth*, Report LR-254, Dept. of Aerospace Engineering, Delft University of Technology, The Netherlands, 1977, pp. 60-83.

[6] Pao, P.S.: **Mechanism of Corrosion Fatigue**, *Fatigue and Fracture*, ASM Handbook, Vol. 19, ASM, S.R. Lampman, ASM International, 1996, pp. 185 - 192.

[7] Hartman, A.: **On The Effect of Oxygen and Water Vapor on the Propagation of Fatigue Cracks in 2024-T3 Alclad Sheet**, *International Journal of Fracture Mechanics*, Vol. 1, No. 3, 1965, pp. 167 - 188.

[8] Broom, T., Nicholson, A.J.: **Atmospheric Corrosion-Fatigue of Age Hardened Aluminum Alloys**, *Journal Institute of Metals*, Vol. 89, 1960, pp. 183 - 190.

[9] Kim, Y.H., Manning, S.D.: **A Superposition Model for Corrosion-Fatigue Crack Propagation in Aluminum Alloys**, *Fracture Mechanics: Fourteenth Symposium-Volume I: Theory and Analysis*, ASTM STP 791, J.C. Lewis and G. Sines, Eds., ASTM, 1983, pp. I-446 - I-462.

[10] Petit, J., Sarrazin-baudoux C., Henaff G.: **An Overview on Environmentally-Assisted Fatigue Crack Propagation**, *FATIGUE '99*, Proc. of The 7th. Int. Fatigue Congress, Vol. 4, Higher Education Press, Beijing, 1999, pp. 2221 - 2228.

[11] Henaff, G., Marchal, K., Petit, J.: **On Fatigue Crack Propagation Enhancement by A Gaseous Atmosphere: Experimental and Theoretical Aspects**, *Acta Metallurgica et Materialia*, Vol. 43, No. 8, 1995, pp. 2931 - 2942.

[12] Enochs, J.S., Devereux, F.: **Fatigue Crack Growth in 5052-H34 Aluminum in Vacuum and Active Gas Environments**, *Metallurgical Transactions A*, Vol. 6A, Feb., 1975, pp. 298 - 304.

[13] Feeney, J.A., McMillan, J.C., Wei, R.P.: **Environmental Fatigue Crack Propagation of Aluminum Alloys at Low Stress Intensity Levels**, *Metallurgical Transactions*, Vol. 1, 1970, pp. 1741 - 1757.

[14] Holroyd, N.J.H., Hardie, D.: **Corrosion fatigue of 7000 Series Aluminum Alloys**, *Environment-Sensitive Fracture: Evaluation and Comparison of Test Methods*, ASTM STO 821, S.W. Dean, E.N. Pugh, and G.M. Ugiansky, Eds., ASTM, Philadelphia, 1984, pp. 534 - 547.

[15] **Standard Test Method for Measurement of Fatigue Crack Growth Rates, ASTM E 647-95a**, *Annual Book of ASTM Standards 1995: Metals Test Methods and Analytical Procedures*, Vol. 03.01., ASTM, USA, 1995, pp. 565 - 601.

[16] **Standard Specification for Substitute Ocean Water, ASTM D1141-90**, *Annual Book of ASTM Standards 1990*, Vol. 11.01., ASTM, USA, 1990, pp. 132 - 133.

[17] Andresen, P.L.: **Corrosion Fatigue Testing**, *Fatigue and Fracture, ASM Handbook*, Vol. 19, ASM International, i997, pp. 193 - 209.

[18] Zuidema, Jan: **Square and Slant Fatigue Crack Growth in Al 2024**, *PhD Dissertation*, Delft University of Technology, Delft, 1995.

[19] McEvily, A.J., Wei, R.P.: **Fracture Mechanics and Corrosion Fatigue**, *Corrosion Fatigue: Chemistry, Mechanisms and Microstructure*, NACE-2, The University of Connecticut, 1972, pp. 381 - 395

[20] Yokobori, Jr., A.T., Nemoto, T., Okada, K., Sekita, S., Sendo, M.: **Effect of Mg Added, Cold Work Hardening, Aging on the Sensistivity of Corrosion Crack Growth Rate of 5083 Aluminum Alloys**, *Proceedings of Recent Advances in Science and Engineering of Light Metals, RASELM '91*, K. Hirano, H. Okikawa, and K. Ikeda, 1991, pp. 329 - 333.

[21] Wei, R.P.: **Fatigue-Crack Propagation in A High-Strength Aluminum Alloy**, *The International Journal of Fracture Mechanics*, Vol. 4, No. 2, June 1968, pp. 159 - 170.

Appendix

A1. Engineering Drawing of The Specimen (unscaled)

A2. Preparation of The Substitute Ocean Water (ASTM D1141)

A3. Engineering Drawing of The Corrosion Cell (unscaled)

A4. Source Program and Screenshot of The Incremental Polynomial Method (ASTM E647)

A5. Detail Test Parameters of The Specimens

A1. Engineering Drawing of The Specimen (unscaled)

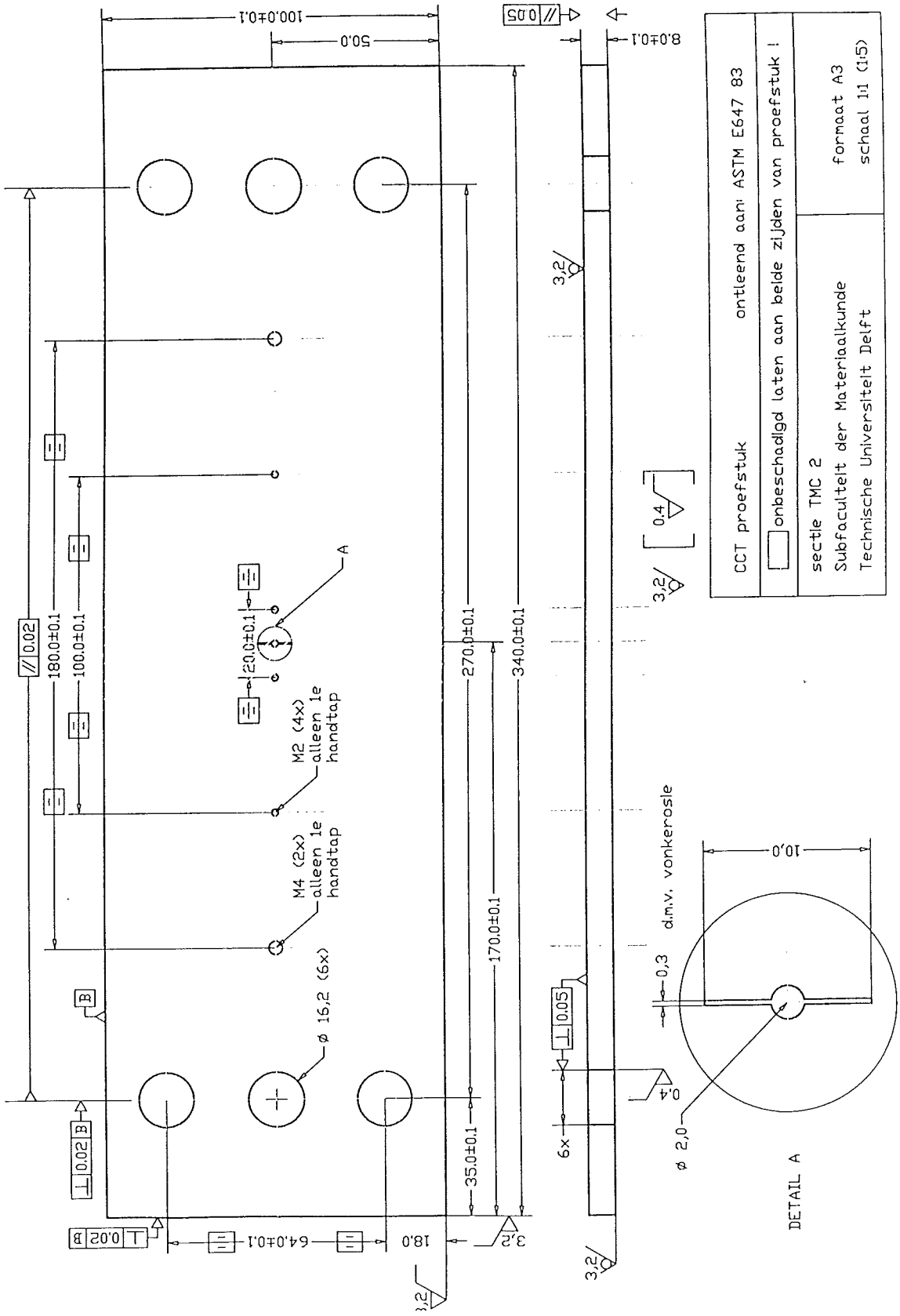

A2. Preparation of The Substitute Ocean Water (ASTM D1141)

In order to make the substitute ocean water, two stock solutions must be prepared first. The stock solutions were prepared as follows:

Stock Solution No. 1

The indicated amount of the following salts was dissolved in water and diluted to a total volume of 7.0 L.

$MgCl_2.6H_2O$	3889.0 g (= 555.6 g/L)
$CaCl_2$ (anhydrous)	405.6 g (= 57 g/L)
$SrCl_2.6H_2O$	14.8 g (= 2.1 g/L)

Stock Solution No. 2

The indicated amount of the following salts was dissolved in water and diluted to a total volume of 7.0 L or a convenient volume.

KCl	486.2 g (= 69.5 g/L)
$NaHCO_3$	140.7 g (= 20.1 g/L)
KBr	70.4 g (= 10.0 g/L)
H_3BO_3	19.0 g (= 2.7 g/L)
NaF	2.1 g (= 0.3 g/L)

To prepare 10.0 L of substitute ocean water, 245.34 g of sodium chloride (NaCl) and 40.94 g of anhydrous sodium sulfate (Na_2SO_4) were dissolved in 8 to 9 L of water. Two hundred mL of Stock Solution No. 1 and 100 mL of Stock Solution No. 2 were added respectively with vigorous stirring. Then, the solution was diluted to 10.0 L. The pH was adjusted to 8.2 with 0.1 M sodium hydroxide (NaOH) solution.

A3. Engineering Drawing of The Corrosion Cell (unscaled)

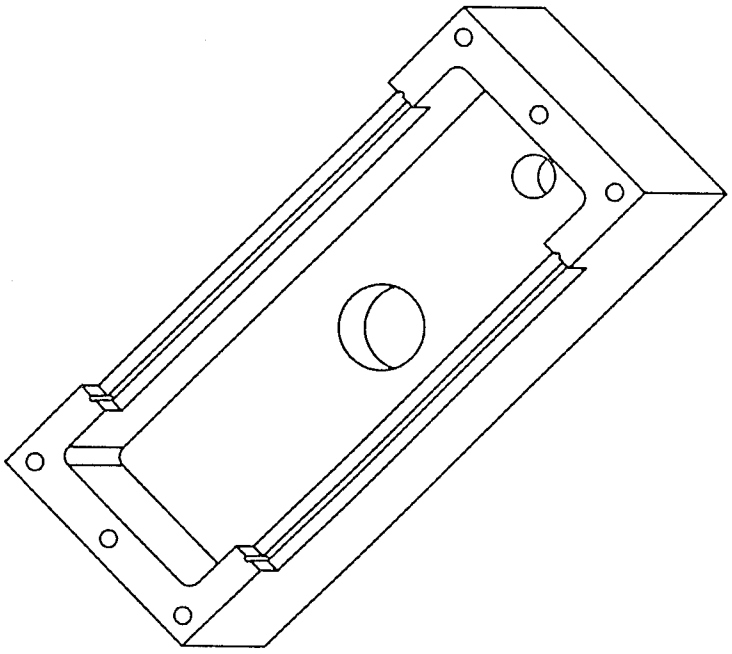

Corrosie cel-deel van perspex voor CCT proefstukken. Twee stuks fabriceren.	
* = volgens bijgeleverde fitting ** = volgens bijgeleverde fitting, gat slechts aan een van de twee cel-delen maken !!!	
Saskia de Vries, sectie MGM (tel : 2229) Subfaculteit der Materiaalkunde Technische Universiteit Delft	formaat A3 schaal 1:1

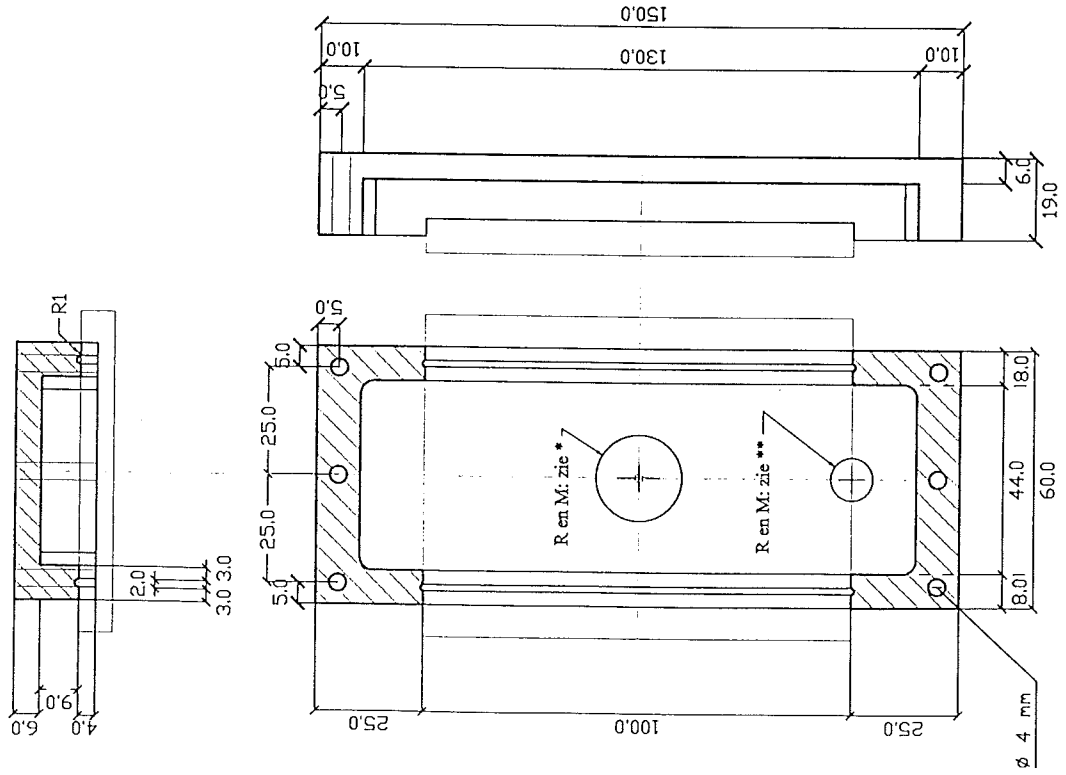

A4. Source Program and Screenshot of The Incremental Polynomial Method (ASTM E647)

The source code for the incremental polynomial method is listed below. The program (poly2.f) is written for FORTRAN 77. For Linux users, there is a graphic user interface (GUI) for the program which is written in Tcl/Tk language. The GUI requires other softwares (poly2.f, gnuplot and gv) to process the data. The output of the program are ASCII text and graphic (postscript). The source code of the GUI is also listed below. The screenshot of the GUI and the output of the program can be seen in Figure 1 and Figure 2.

The source code of the incremental poynomial method (poly2.f):

```
      program dadnvsdK
      character datafile*25,outfile*25,avn*25
      real a,pmax,pmin,da,lower,w,b,ain
      real af,crack(500),load(2,500),p1,p0,ratio,p2
      double precision pi
      integer cycles,n,ni,div,point,ncyc(500),k,eof,dummy
      common /pi/pi
c
      pi=4.0*datan(1.0D+00)
      open(1,file='input.dat')
      read(1,*) datafile
      read(1,*) outfile
      read(1,*)a0,af
      read(1,*)point
      read(1,*)b,w
      read(1,*)p2,p1,p0,ratio
      close(1)
      open(3,file=datafile)
      open(4,file=outfile,status='unknown')
      open(6,file='curve.gnu',status='unknown')
      rewind(3)
      i=1
      j=1
      if (point.ne.0) then
              point=point+6
              div=point
              da=(af-a0)/div
      end if
      DO WHILE (EOF.ne.-1)
              read(3,*,end=40) cycles,a,pmax,pmin
c             read(3,*,end=40) cycles,dummy,a,pmax,pmin
              if (point.ne.0) then
                      lower=a0+da*(i-1)
              else
                      lower=a0
              end if
              if ((a.ge.lower).and.(a.le.af)) then
                      ncyc(i)=cycles
                      crack(i)=a
                      load(1,i)=pmax
                      load(2,i)=pmin
              i=i+1
              end if
      END DO
40    k=i-1
      call polynom(crack,ncyc,k,load,w,b,p2,p1,p0,ratio)
      close(3)
      close(4)
```

```
      close(5)
      close(6)
      end
c
      subroutine polynom(a,n,npts,load,w,b,p2,p1,p0,ratio)
      real a(500),bb(3),dadn(500),delk(500),id(7),aa(10)
      real load(2,500),c1,c2,sx,sx2,sx3,sx4,sy,syx,syx2
      real x,yy,den,t2,t3,t4,yb,rss,tss,yhat,r2,ar,s,t,w
      real sec,ft,pmax,pp,ax,ratio,pmin,p1,p0,u,p2
      double precision pi
      integer n(500),nn(10),npts,i,l,k,k1,j,qq
      common /pi/pi
c
      npts=npts-6
      k=0
      do 100 i=1,npts
            l=0
            k=k+1
            k1=k+6
            pmax=0.
            pmin=0.
c           pp=pp*1000.
            do 60 j=k,k1
                  l=l+1
                  aa(l)=a(j)
                  nn(l)=n(j)
                  pmax=pmax+load(1,j)
                  pmin=pmin+load(2,j)
60          continue
            pmax=pmax/l
            pmin=pmin/l
            pp=pmax-pmin
            c1=0.5*(nn(1)+nn(7))
            c2=0.5*(nn(7)-nn(1))
            sx=0
            sx2=0
            sx3=0
            sx4=0
            sy=0
            syx=0
            syx2=0
            do 70 j=1,7
                  x=(nn(j)-c1)/c2
                  yy=aa(j)
                  sx=sx+x
                  sx2=sx2+x**2
                  sx3=sx3+x**3
                  sx4=sx4+x**4
                  sy=sy+yy
                  syx=syx+x*yy
                  syx2=syx2+yy*x**2
70          continue
            den=7.0*(sx2*sx4-sx3**2)-sx*(sx*sx4-sx2*sx3)+
     #sx2*(sx*sx3-sx2**2)
            t2=sy*(sx2*sx4-sx3**2)-syx*(sx*sx4-sx2*sx3)+
     #syx2*(sx*sx3-sx2**2)
            bb(1)=t2/den
            t3=7.0*(syx*sx4-syx2*sx3)-sx*(sy*sx4-syx2*sx2)+
     #sx2*(sy*sx3-syx*sx2)
            bb(2)=t3/den
            t4=7.0*(sx2*syx2-sx3*syx)-sx*(sx*syx2-sx3*sy)+
     #sx2*(sx*syx-sy*sx2)
            bb(3)=t4/den
            yb=sy/7.0
            rss=0
```

```
                tss=0
                do 75 j=1,7
                        x=(nn(j)-c1)/c2
                        yhat=bb(1)+bb(2)*x+bb(3)*x**2
                        rss=rss+(aa(j)-yhat)**2
                        tss=tss+(aa(j)-yb)**2
75              continue
                r2=1.0-rss/tss
                dadn(i)=bb(2)/c2+2.0*bb(3)*(nn(4)-c1)/c2**2
                x=(nn(4)-c1)/c2
                ar=bb(1)+bb(2)*x+bb(3)*x**2
                s=1.0e+10
                snet=0
                qq=i+3
                t=2.0*ar/w
                sec=1.0/(cos(pi*t/2.0))
                ft=sqrt((pi*t*sec)/2.0)
                delk(i)=(ft*pp)/(b*sqrt(w))
                delk(i)=sqrt(1.e-3)*delk(i)
                u=p2*ratio**2+p1*ratio+p0
                dkeff=delk(i)*u
                write(4,*) ar,n(qq),r2,delk(i),dkeff,dadn(i)
100     continue
        end
```

The source code of the GUI:

```
#! /usr/X11R6/bin/wish8.0
#
wm title . TKFatigue

frame .zero
frame .one
frame .onea
frame .oneb
frame .onec
frame .oned
frame .two
pack .zero -side top -fill x -ipadx 5
pack .one -side top -fill x -ipadx 5 -ipady 5
pack .onea -side top -fill x -ipadx 5
pack .oneb -side top -fill x -ipady 5
pack .onec -side top -fill x -ipady 5
pack .oned -side top -fill x -ipady 5
pack .two -side top -fill x -ipady 5

label .zero.lbl1 -text {This software is created by a person}
pack .zero.lbl1 -padx 5
label .zero.lbl2 -text {who is smarter than you}
pack .zero.lbl2 -padx 5
label .zero.lbl -text {General :}
pack .zero.lbl -side left -padx 5

foreach field {{Input file} {da/dN vs delta K file} {Graphic File}
{Initial crack length [mm]} {Final crack length [mm]} {Number of points}} {
label .one.l$field -text $field -font helvetica
entry .one.e$field -textvariable lines($field) -relief sunken -bg pink -fg\
darkred
grid .one.l$field .one.e$field
grid .one.l$field -sticky w
grid .one.e$field -sticky e
}

label .onea.specimen -text {Specimen :}
```

```
pack .onea.specimen -side left -padx 5

foreach field {{Thickness [mm]             } {Width [mm]}} {
label .oneb.l$field -text $field -font helvetica
entry .oneb.e$field -textvariable lines($field) -relief sunken -bg pink -fg\
darkred
grid .oneb.l$field .oneb.e$field
grid .oneb.l$field -sticky w
grid .oneb.e$field -sticky e
}

label .onec.lbl -text {Crack Closure Formula :}
pack .onec.lbl -side left -padx 5

foreach field {{P0} {P1} {P2} {Stress ratio                    }} {
label .oned.l$field -text $field -font helvetica
entry .oned.e$field -textvariable lines($field) -relief sunken -bg pink -fg\
darkred
grid .oned.l$field .oned.e$field
grid .oned.l$field -sticky w
grid .oned.e$field -sticky e
}

button .two.run -text Run -command Run
button .two.quit -text Quit -command exit
pack .two.run -side left -padx 10
pack .two.quit -side right -padx 10
bind .two.run <Return> Run
bind .two.quit <Return> exit

proc Run {} {
        global lines
#
# write a file for poly2
#
        set fileId [open input.dat w 0666]
        puts $fileId $lines(Input file)
        puts $fileId $lines(da/dN vs delta K file)
        set aiaf $lines(Initial crack length \[mm\])
        append aiaf " "
        append aiaf $lines(Final crack length \[mm\])
        puts $fileId $aiaf
        puts $fileId $lines(Number of points)
        set bw $lines(Thickness \[mm\]             )
        append bw " "
        append bw $lines(Width \[mm\])
        puts $fileId $bw
        set coeff $lines(P2)
        append coeff " "
        append coeff $lines(P1)
        append coeff " "
        append coeff $lines(P0)
        append coeff " "
        append coeff $lines(Stress ratio                    )
        puts $fileId $coeff
        close $fileId
#
# write a file for gnuplot
#
        set fileId1 [open curve.gnu w 0666]
        puts $fileId1 "set key left top"
        puts $fileId1 "set logscale x"
        puts $fileId1 "set logscale y"
        puts $fileId1 "set xlabel 'delta K \[MPa.m^{1/2}\]'"
        puts $fileId1 "set ylabel 'da/dN \[mm/cycle\]'"
```

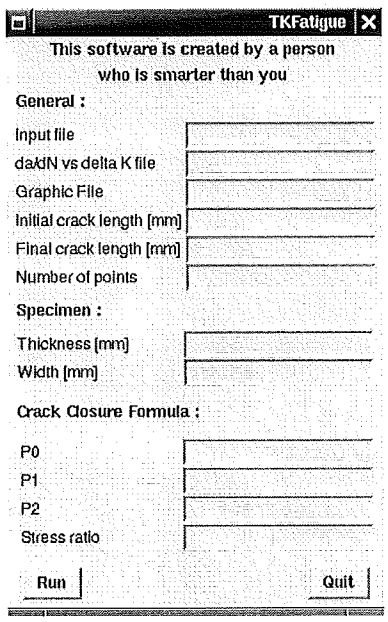

Figure 1: Screenshot of the GUI running on Linux.

```
        puts $fileId1 "set grid xtics mxtics ytics mytics lt 5"
        puts $fileId1 "set title ' '"
        puts $fileId1 "set terminal postscript landscape enhanced \\"
        puts $fileId1 "color solid 'Helvetica' 12"
        set dummy "set output '"
        append dummy $lines(Graphic File)
        append dummy "'"
        puts $fileId1 $dummy
        set dummy1 "plot '"
        append dummy1 $lines(da/dN vs delta K file) "' using 4:6 title 'delta K' \\"
        puts $fileId1 $dummy1
        set dummy2 "#, '"
        append dummy2 $lines(da/dN vs delta K file) "' using 5:6 title 'delta K_{eff}'"
        puts $fileId1 $dummy2
        close $fileId1
# execute poly2
        exec poly2
# execute gnuplot
        exec gnuplot curve.gnu
# execute gv to view the graph
        exec gv $lines(Graphic File)
        exit
}
```

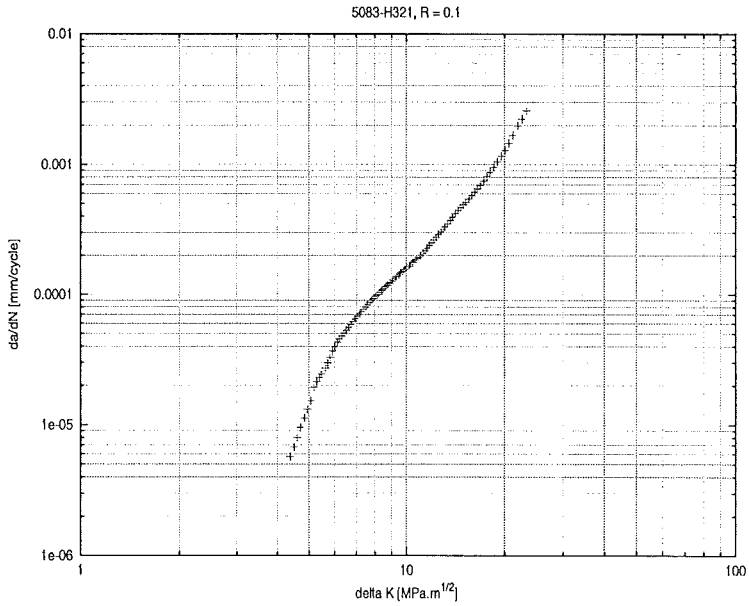

Figure 2: Typical postscript output of the program.

A5. Detail Test Parameters of The Specimens

SPECIMEN CODE	TEST	PRE-CRACK	FATIGUE CRACK	RE-MARK
Calibr2	calibration, T-L, f=10 Hz, R=0.5, lab air	-	ΔK=7 MPa$\sqrt{m}$	1)
CALIB-1	calibration, L-T, f=10 Hz, R=0.5, lab air	-	ΔK=7 MPa$\sqrt{m}$	1)
AIR-1	CA, lab air, T-L, R=0.5	P_{max}=42 kN, a=5-6 mm f=20 Hz	P_{max}=35 kN, a $\geq$6 mm f=10 Hz	
AIR-2	CA, lab air, T-L, R=0.1	P_{max}=42 kN, a=5-6 mm f=20 Hz	P_{max}=35 kN, a $\geq$6 mm f=10 Hz	
AIR-3	CA, lab air, T-L, R=0.1	P_{max}=30 kN, a=5-6 mm f=20 Hz	P_{max}=25 kN, a $\geq$6 mm f=10 Hz	
AIR-4	CA, lab air, T-L, R=0.5	P_{max}=42 kN, a=5-6 mm f=20 Hz	P_{max}=25 kN, a $\geq$6 mm f=10 Hz	
AIR-5	CA, alt. freq. 10 & 0.1 Hz, lab air, R=0.1	P_{max}=42 kN, a=5-6 mm f=20 Hz	P_{max}=35 kN, f=10 Hz, 6<a$\leq$13 mm f=0.1 Hz, 13<a$\leq$17 mm f=10 Hz, 17<a$\leq$27 mm f=0.1 Hz, 27<a$\leq$35 mm f=10 Hz, 35<a$\leq$42 mm	
CA1	CA, lab air, L-T, R=0.1	P_{max}=30 kN, a=5-6 mm f=20 Hz	P_{max}=25 kN, a $\geq$6.3 mm f=10 Hz	
CA3	CA, lab air, L-T, R=-0.25	P_{max}=30 kN, a=5-6.4 mm f=20 Hz	P_{max}=25 kN, a $\geq$6.4 mm f=10 Hz	2)
CA4	CA, lab air, L-T, R=-0.25	P_{max}=30 kN, a=5-7.2 mm f=20 Hz	P_{max}=25 kN, a $\geq$7.2 mm f=10 Hz	
CA5	CA, lab air, L-T, R=-1	P_{max}=30 kN, a=5-7 mm f=15 Hz	P_{max}=30 kN, a$\geq$7 mm f=10 Hz	
CA6	CA, lab air, L-T, R=0.5	P_{max}=42 kN, a=5-8 mm f=15 Hz	P_{max}=40 kN, a$\geq$8 mm f=10 Hz	
pmaxpm3	IA, lab air, L-T, R=0.1, f= 10 Hz	P_{max}=42 kN, a=5-7 mm Load shedding with $1/K.dK/da \geq -0.8$, a=7-10 mm	see Figure 3.8	3)
pmaxpm5	IA, lab air, L-T, R=0.1, f=10 Hz	P_{max}=42 kN, a=5-7 mm Load shedding with $1/K.dK/da \geq -0.8$, a=7-10 mm	see Figure 3.8	3)

SW1	CA, seawater, L-T, R=0.1	f=10 Hz P_{max}=44 kN, a=5-6.3 mm P_{max}=37.5 kN, a=6.3-6.8 mm P_{max}=30 kN, a=6.8-7.2 mm	P_{max}=25 kN, a≥7.2 mm f=10 Hz	4)
SW3	IA, seawater, L-T, R=0.1	P_{max}=30 kN, a=5-7.5 mm f=20 Hz	see Figure 3.10 f=10 Hz	
SW4	IA, seawater, L-T, R=0.1	f=20 Hz P_{max}=30 kN, a=5-6.4 mm P_{max}=25 kN, a=6.4-6.9 mm	see Figure 3.11 f=1 Hz	
SW6	CA, seawater, L-T, R=0.1	f=20 Hz P_{max}=35 kN, a=5-7 mm P_{max}=30 kN, a=7-8 mm	P_{max}=25 kN, a≥8 mm f=1 Hz	5)
SW7	CA, seawater, L-T, R=0.1	P_{max}=30 kN, a=5-13 mm f=20 Hz	P_{max}=28 kN, a≥13 mm f=1 Hz	
SW8	CA, seawater, L-T, R=0.5	P_{max}=50 kN, a=5-7 mm f=15 Hz	P_{max}=45 kN, a≥7 mm f=1 Hz	
SW9	CA, seawater, L-T, R=0.5	P_{max}=50 kN, a=5-7.7 mm f=15 Hz	P_{max}=45 kN, a≥7.7 mm f=1 Hz	
SW11	CA, seawater, L-T, R=0.1	P_{max}=32 kN, a=5-7 mm f=20 Hz	P_{max}=32 kN, a≥7 mm f=1 Hz	
SW13	IA, seawater, L-T, R=0.1	P_{max}=32 kN, a=5-7 mm f=20 Hz	see Figure 3.13 f=1 Hz	
SW14	CA, seawater, L-T, R=0.1	P_{max}=40 kN, a=5-7 mm f=20 Hz	P_{max}=35 kN, a≥7 mm f=1 Hz	
SW15	IA, seawater, L-T, R=0.1	P_{max}=32 kN, a=5-7 mm f=20 Hz	see Figure 3.13 f=1 Hz	
SW16	IA, seawater, L-T, R=0.1	P_{max}=32 kN, a=5-7 mm f=20 Hz	see Figure 3.12 f=1 Hz	
SW17	IA, seawater, L-T, R=0.5	P_{max}=46 kN, a=5-9 mm f=25 Hz	see Figure 3.14 f=1 Hz	

Remarks:

1) Constant ΔK test
2) Interrupted at a = 10.7 mm
3) After the IA test there was a series of other tests, but it was beyond the scope of the thesis
4) Accidentally overloaded at the beginning of the test with $P \approx 60$ kN
5) Visual crack length measurement